The Dissertation Committee for Bangguo Xiong
certifies that this is the approved version of the following dissertation:

Toward a Geometric Theory of Magnetization Dynamics: Electronic Contribution in the Semiclassical Approach

Committee:

Qian Niu, Supervisor

Allan H. MacDonald

Alexander A. Demkov

Chih-Kang Shih

Emanuel Tutuc

Toward a Geometric Theory of Magnetization Dynamics: Electronic Contribution in the Semiclassical Approach

by

Bangguo Xiong

DISSERTATION

Presented to the Faculty of the Graduate School of

The University of Texas at Austin

in Partial Fulfillment

of the Requirements

for the Degree of

DOCTOR OF PHILOSOPHY

THE UNIVERSITY OF TEXAS AT AUSTIN

May 2019

Dedicated to my family.

Acknowledgments

I would like to express my sincere gratitude to my advisor Dr. Qian Niu, for the continuous support of my Ph.D study, for his patience, motivation and immense knowledge. His sharp mind always saves me when I get stuck in my research. With his guidance, I do not get lost in the oceans of formulas and codes that often. I could not have imagined having a better advisor in the journey of exploring new knowledge.

I would like to thank Dr. Hua Chen, for his tremendous help in my first paper. From him I learned most of the professional skills as a scholar.

I would like to extend my appreciation to all the other members on my graduate committee, Dr. Allan H. MacDonald, Dr. Alexander A. Demkov, Dr. Chih-Kang Shih and Dr. Emanuel Tutuc, for providing critical suggestions in writing this dissertation.

My thanks also go to Ervin Matthew, Carol Monette and Dr. John Keto, for all their invaluable advices on the graduate stuff during these years.

I would like to thank all the members in the Niu's group during my time here, Ran Cheng, Xiao Li, Yang Gao, Lifa Zhang, Cong Xiao, Hailong Zhou, Liang Dong, JingJing Feng, Daniyar Saparov, Qiang Gao, Xiao Li, Haodi Liu and Kaige Hu. In my first year, Ran taught me a lot on the Berry phase effects. Lifa introduced me to the field of topological phonon as my first

research project, which I presented for my Ph.D qualifier. I am very grateful to their help. The group lunch with them is one of the best times every week.

Finally, I would like to thank my parents and my love of life with all my heart. Their love and support help me get through the toughest time of my Ph.D life.

Toward a Geometric Theory of Magnetization Dynamics: Electronic Contribution in the Semiclassical Approach

Publication No. _____

Bangguo Xiong, Ph.D.
The University of Texas at Austin, 2019

Supervisor: Qian Niu

This dissertation presents theoretical studies of the magnetization dynamics in ferromagnetic materials. To give a general description of the influences of electric fields or currents on magnetization dynamics, we developed a semiclassical theory for the magnetization implicitly coupled to electronic degrees of freedom. In the absence of electric fields, the Bloch electron Hamiltonian changes the Berry curvature, the effective $\boldsymbol{H}$ fields and the damping in the dynamical equation of the magnetization, which we classify into intrinsic and extrinsic effects. Static electric field modifies these as first-order perturbations, with which we are able to give a physically clear interpretation of the current-induced spin-orbit torques.

In analogy of the electromagnetic fields, the Berry curvature is the *magnetic field* and the gradient of energy is the *static electric field* in the magnetization space. If the system is driven by external forces, an additional Faraday

$\boldsymbol{H}$ field appears. The Faraday $\boldsymbol{H}$ field can be provided by electron motion, e.g. in the presence of electric fields, giving the intrinsic spin-orbital torque. We use a toy model mimicking a ferromagnet-topological-insulator interface to illustrate the various effects, and we predict an anisotropic gyromagnetic ratio and the dynamical stability for an in-plane magnetization.

In the presence of inhomogeneity, the Faraday $\boldsymbol{H}$ field can be provided by electron velocity, giving rise to the intrinsic spin-transfer torque. In the semiclassical framework, the electronic spin dipole is found to influence the magnetization dynamics in terms of Dzyaloshinskii-Mariya interaction. We obtain both the equilibrium spin dipole and the field-induced spin dipole, for the equilibrium and non-equilibrium Dzyaloshinskii-Mariya interaction, respectively. In addition, the induced effective $\boldsymbol{H}$ field has a geometric contribution in the second Chern form, extending the first Chern form in uniform systems. Our results provide methods for the electric field control of magnetic structures.

Table of Contents

List of Tables

List of Figures

Chapter 1

Introduction

1.1 Motivation and Outline

Magnetization is a fundamental physical quantity in solid states. It describes the circular motion of charge and the polarization of spin in magnetic materials, and determines the electromagnetic responses of the medium. In modern technology applications, magnetic materials, such as magnetic films and particles, are the building blocks of the devices for information processing and storage. The field of spintronics seeks to understand the coupling between carrier electrons and magnetization, and hence provides guidance for designing devices with better performance in energy efficiency and operation speed.

Magnetization-dependent transport and current-induced torque (CIT) are two reciprocal aspects of the interplay between carrier electrons and magnetization, for example, the Giant MagnetoResistance (GMR) effect and the Spin-Transfer Torque (STT). Information is written into the device by applying a current that changes the magnetization status via the STT. On the other hand, information is read out by measuring the electric resistance via the GMR effect. Our focus in this work is on the aspect of the current-induced torques. The reciprocal relation between them provides guidance in exploring

the various mechanisms in spin torques from the other perspective.

From the theoretical aspect, two mainstream methods on the CIT have been developed: the phenomenological theory based on the current and spin transport [6, 7, 8], and the Kubo formula in the framework of linear response theory [9, 10, 11]. The phenomenological theory has the advantage of a relative simple picture, and is able to provide a quick access to the interesting physics even in complicated magnetic structures. However, parameters in the phenomenological theory should be obtained from experimental results. On the other hand, the Kubo formula methods require no external inputs. It can start from an *ab* initial calculation and calculate the response coefficients of spin torques, though complicated expressions are often involved in the numerical evaluations.

In this dissertation, we present a semiclassical framework for the magnetization dynamics, where the CIT is derived using the wavepacket methods of electrons. The wavepacket has a center position and center momentum, as an analogy of classical objects [12]. The evolution of the wavepacket follows the classical mechanics, where the quantum mechanical effects are included by the Berry phase. The semiclassical formalism extracts the information of energy and Berry curvature from the Bloch bands of electrons, providing quantitatively good results.

The dissertation naturally breaks into two parts, the spin torques in uniform magnetic materials, and the spin torques in materials with inhomogeneity. In Chapter two, the magnetization dynamics for uniform magnetic

materials is introduced, and the electric field-induced effects on the Landau-Lifshitz-Gilbert equation are discussed. As examples, the ferromagnets in contact with 3D and 2D topological insulators are discussed, respectively, revealing the special role of the Faraday $\boldsymbol{H}$ field. In Chapter three, the semiclassical theory is extended to inhomogeneous magnetic materials using the second-order wavepacket methods. The effective $\boldsymbol{H}$ field from the electronic contribution includes the Dzyaloshinskii-Moriya Interaction (DMI) and the second Chern form for ferromagnetic insulators. We use a transition-metal-dichalcogenide/ferromagnets heterostructure to show the field-induced effects.

In the following sections in this chapter, some background knowledge and conventions are introduced.

1.2 Magnetization Dynamics

We first gives a clear definition of the magnetization. In history, electrons in the medium are separated as bound electrons and itinerant electrons, as a preliminary understanding of the insulating and conducting behaviors. Magnetization and polarization are used to describe the bound electrons. However, the separation of the bound and itinerant electrons is a vague concept that needs to be refined. In the band theory of solids, polarization in insulators is built on the adiabatic charge transportation [13], and the concept of bound electrons is discarded.

The modern theory of magnetization is developed by D. Xiao *et al.* and J. Shi *et al.*, from the thermal dynamical point of view using the semiclassical

methods and the quantum mechanical methods, respectively [14, 15]. For systems in equilibrium, the magnetization is defined by taking the derivative in magnetic field for the free energy density,

$$\boldsymbol{m} = -\partial G/\partial \boldsymbol{B}, \tag{1.1}$$

where G represents the free energy in the presence of $\boldsymbol{B}$ field. This definition takes all electrons on equal foot and is applicable to insulators and metals, as long as the electrons are in equilibrium. The magnetization expression they obtained contains the orbital contribution only, while the conventional spin magnetization is regarded as the orbital magnetization for the Dirac electrons. The Berry curvature of the Bloch electrons gives the intercell part of the orbital magnetization, which has the same origin as the Hall current. It can be alternatively understood in terms of edge currents in a finite-size system. The intracell part of the orbital magnetization is from the current circulation within the unit cell.

In crystals, the spin magnetization is dominant over the orbital magnetization. The reason is that the spatial rotation symmetry is broken by the anisotropic interaction with the lattices, and thus the orbital magnetization is quenched. In the semiclassical framework, the magnetization is regarded as a general order parameter. The origin of magnetization only matters when its coupling to carriers are concerned. We take the *sd* type coupling for simplicity, though more general coupling form is allowed.

1.2.1 The Laundau-Lifshitz-Gilbert Equation

The classical theory describing the magnetization dynamics of ferromagnetic materials started from Landau and Lifshitz [16, 17]. The spin magnetic momentum is related to the spin angular momentum by the gyromagnetic ratio, $\boldsymbol{M} = -\gamma \boldsymbol{S}$, where $\gamma = g_s \mu_B / \hbar$. The angular momentum is driven by the torque in a magnetic field $\boldsymbol{H}$, $\boldsymbol{T} = \boldsymbol{M} \times \boldsymbol{H}$. Thus the dynamics of magnetic momentum is,

$$\dot{\boldsymbol{M}} = -\gamma \boldsymbol{M} \times \boldsymbol{H}. \tag{1.2}$$

The magnetization motion couples with other excitations in solids, e.g. lattice vibration, spin waves, eddy currents and impurities. The coupling tends to relax the magnetization along the direction of lowest energy. Phenomenologically, the relaxation is described by the damping term according to Landau and Lifshistz,

$$\dot{\boldsymbol{M}} = -\gamma \boldsymbol{M} \times \boldsymbol{H} - \lambda \boldsymbol{M} \times (\boldsymbol{M} \times \boldsymbol{H}). \tag{1.3}$$

where λ is the damping parameter. However, the above equation fails to fit experiments with a satisfying damping and gyromagnetic ratio in the thin ferromagnetic sheets with large damping effects. To obtain a more effective damping form, Gilbert found an alternative way to introduce the damping by the Rayleigh dissipation functional [18],

$$R = \frac{\eta}{2} \int \dot{\boldsymbol{M}} \cdot \dot{\boldsymbol{M}} dr, \tag{1.4}$$

where η is the Rayleigh constant. The damping field $-\eta\dot{\boldsymbol{M}}$ is added to the magnetic field $\boldsymbol{H}$ in the equation of motion,

$$\dot{\boldsymbol{M}} = -\gamma \boldsymbol{M} \times (\boldsymbol{H} - \eta\dot{\boldsymbol{M}}). \tag{1.5}$$

The new effective gyromagnetic ratio and damping coefficient are renormalized as,

$$\gamma' = \frac{\gamma}{1 + \gamma^2\eta^2 M_s^2}, \tag{1.6}$$

and

$$\lambda = \frac{\gamma^2\eta}{1 + \gamma^2\eta^2 M_s^2}. \tag{1.7}$$

The LLG equation solves the issue in the large damping regime. In the small λ limit, these two forms of magnetization dynamics are equivalent in the linear order.

1.2.2 The Niu-Kleinman Equation

The magnetization dynamics can not be derived from the Lagrangian consisting of the kinetic energy and the potential energy. The fundamental reason is that the commutation relation of the angular momentums can not be captured. In fact, magnetization dynamics does not have a kinetic energy, and a geometry phase determines the dynamical structure of magnetization. The geometric phase originates from the electronic wavefunction that depends on magnetization. Niu and Kleinman [19] considered an adiabatic evolution of the electronic states on the manifold of lowest energy. The Lagrangian of the electronic wavefunction is $\mathcal{L} = \langle\Phi|i\hbar\partial_t - \hat{H}|\Phi\rangle$, which is equivalent to the

Schordinger equation on the manifold. The electronic degrees of freedom is integrated out to obtain the effective Lagrangian of magnetization,

$$\begin{aligned} \mathcal{L} &= \langle \Phi | i\hbar \dot{\boldsymbol{m}} \frac{\partial}{\partial \boldsymbol{m}} - \hat{H} | \Phi \rangle, \\ &= \hbar \dot{\boldsymbol{m}} \cdot A_{\boldsymbol{m}} - E_0(\boldsymbol{m}), \end{aligned} \tag{1.8}$$

where the Berry connection $A_{\boldsymbol{m}} = \left\langle \Phi | i\partial_{\boldsymbol{m}} | \Phi \right\rangle$ and E_0 is the lowest energy for the electronic states with the constraint $\boldsymbol{m} = \left\langle \Phi | \hat{m} | \Phi \right\rangle$. Applying the Lagrangian principle, Niu and Kleinman obtained the following equation of motion,

$$\hbar \Omega_{\boldsymbol{mm}} \dot{\boldsymbol{m}} - \frac{\partial E_0}{\partial \boldsymbol{m}} = 0, \tag{1.9}$$

where $\Omega_{m_i m_j} = \partial_{m_i} A_{m_j} - \partial_{m_j} A_{m_i}$ is the Berry curvature. The Niu-Kleinman equation can be recasted into the LLG equation by defining the gyromagnetic ratio,

$$\hbar \vec{\Omega}_m = \frac{\vec{m}}{\gamma m^2}. \tag{1.10}$$

For example, the gyromagnetic ratio of the electronic spin [20] is $\gamma = g_s \mu_B / \hbar$, where the Land factor $g_s = 2$. This result can be obtained by the Berry curvature $\vec{\Omega}_m = \vec{m}/2m^3$ in the $\vec{m} \cdot \vec{\sigma}$ model.

The Berry phase term in the Lagrangian incorporates the commutation relation between the magnetization components, changing the canonical structures in the magnetization space. However, the adiabatic dynamical equation misses the damping terms in the LLG equation: No energy dissipation mechanism is included in the adiabatic approximation.

1.3 Semiclassical Dynamics of Electrons

In a perfect solid, electrons are described by the Bloch states, which are eigenstates of the electronic Hamiltonian. As time evolves, electrons stay on the Bloch states and acquire a dynamical phase, i.e. the time integral of energy. In the presence of perturbations, electrons are scattered between the Bloch states, and the time evolution can be complicated depending on the form of perturbations. The semiclassical methods are aimed to solve the evolution of electrons in the presence of a *slowly varying* perturbation. In the spirit of semiclassical methods, one seeks to understand the quantum evolution with a classical analogy. The wavepacket is a crucial object that mediates the transition from the quantum to the classical language.

1.3.1 Wavepacket Dynamics

The wavepacket is well localized around center position x_c, and the size of the wavepacket is smaller than the typical length scale of perturbation. The local Hamiltonian H_c is evaluated at the center position. The Bloch states of the local Hamiltonian $\psi_{np} = e^{ipx}|u_{np}(x)\rangle$ are used to construct the wavepacket,

$$|W\rangle = \int [dp] C(p) |\psi_{np}\rangle, \tag{1.11}$$

where $C(p)$ is the coefficient and n is the band index. The wavepacket also has a center momentum p_c, with $|C|^2 \approx \delta(p - p_c)$. The center position of the wavepacket is calculated self-consistently,

$$x_c = \langle W|\hat{x}|W\rangle = -\frac{\partial \phi}{\partial p} + A_p, \tag{1.12}$$

where the Berry connection is defined on the periodic part of Bloch states $A_p = \langle u|i\partial_p|u\rangle$, ϕ is the phase of coefficient $C = |C|e^{i\phi}$. These quantities are all evaluated at the center momentum p_c.

Naively, the evolution of wavepacket is determined by its components, each of which evolves independently according to the Schordinger equation. To obtain the velocity of wavepacket, the center position is reevaluated after infinitesimal time δt. However, the local Hamiltonian that governs the wavepacket evolution is time dependent, explicitly or implicitly via the wavepacket center position. In addition, the crystal momentum is varying in time, contributing a time dependence in the Hamiltonian $H_p = e^{ipx}H_c e^{-ipx}$. The time dependence of Hamiltonian renders that the methods of evaluating the velocity operator average are accurate only in the zeroth order of external perturbations, $\dot{\hat{r}} = [\hat{r}, \hat{H}_c]/i\hbar + O(1)$.

The evolution picture also puts a requirement on the wavepacket description: the wavepacket can not lose the localization in space before making a collision with impurities, i.e. $\omega\tau > 1$, where ω is the collision frequency and τ is the time scale of the localization. τ is limited by the coherence time τ_c and the dynamical phase acquired in the evollution, represented by τ_d. Because the decoherence happens after one collision at least, $\omega\tau_c > 1$ is alway satisfied. τ_d is determined by the momentum width of wavepacket Δp with $\tau_d \partial\varepsilon/\partial p \cdot \Delta p = \hbar$. On the other hand, the collision frequency ω is porportional to the density of impurities. Therefore, for dirty samples with flat bands the wavepacket representation is more valid. After a collision, a new electron wavepacket is

constructed at the same position and continues the evolution.

In the limit of weak spatial gradients, the Bloch states evolve according to the adiabatic theorem. The limit requires that $\hbar v_0/E_{gap}l < 1$, where v_0 is the electron velocity, l is the typical length of the spatial gradient and E_{gap} denotes the electronic band gap. For the adiabatic evolution, the probability distribution on the electronic states stays the same, and a Berry phase is acquired in addition to the dynamical phase. After an infinitesimal time δt, the wavepacket evolves to,

$$|W(t+\delta t)\rangle = \int [dp] C_0(p) e^{-i(\varepsilon \delta t - A_p \delta p - A_x \delta x_c - A_t \delta t)} |\psi(p+\delta p, x_c + \delta x_c, t+\delta t)\rangle. \tag{1.13}$$

Note both the variations in crystal momentum p and time t are considered. One can reevaluate the center position and obtain the velocity of wavepacket as,

$$\dot{x} = \frac{\partial \varepsilon}{\partial p} - \Omega_{pp}\dot{p} - \Omega_{px}\dot{x} - \Omega_{pt}. \tag{1.14}$$

The velocity of wavepacket can also be obtained by evaluating the velocity operator average. However, the wavepacket should be calculated beyond the adiabatic evolution theorem: The probability distribution should be kept to the linear order. Although the phase is accurate in the first order in the adiabatic theorem, it is only a gauge effect and does not manifest itself in evaluating the operator averages. This reasoning on the orders of phase and probability teaches us that, to derive the second-order effects, one should use the second-order Berry phase with the first-order probability, or directly use

the second-order probability.

An equivalent representation of the Schordinger equation on the wavefunction evolution is the Lagrangian methods. For any wavefunction $|W\rangle$, consider the Lagrangian, $\mathcal{L} = \langle W|i\frac{d}{dt} - \hat{H}|W\rangle$. Then the Schordinger equation is recovered by applying the Lagrangian principle and taking the derivative with respect to the conjugate wavefunction $\langle W|$. The adiabatic evolution can be obtained by applying the constraint: The wavefunction is confined in one band. Note the variation of wavefunction is only in the one-band manifold, instead of the whole Hilbert space. Hence the wavefunction loses the components in the quotient space in other bands. Notably, the order of the Berry phase effect is one order higher than that of the base manifold. This justifies our usage of the zeroth-order manifold in the first-order theory, and the linear-order manifold in the second-order theory. The Lagrangian of wavepacket is derived as,

$$\mathcal{L} = -\frac{\partial\phi}{\partial t} + \dot{x}A_x + A_t - \varepsilon, \tag{1.15}$$

where the Berry connection $A_x = \langle u|i\partial_x|u\rangle$ and $A_t = \langle u|i\partial_t|u\rangle$, ε is the wavepacket energy. To obtain the Lagrangian for wavepacket, one replaces the ϕ phase term with the center position,

$$\mathcal{L} = \dot{p}(-x + A_p) + \dot{x}A_x + A_t - \varepsilon, \tag{1.16}$$

Applying the Lagrangian principle, a set of equations of motion for wavepack-

ets is obtained,

$$\dot{x} = \frac{\partial \varepsilon}{\partial p} - \Omega_{pp}\dot{p} - \Omega_{px}\dot{x} - \Omega_{pt}, \tag{1.17}$$

$$\dot{p} = -\frac{\partial \varepsilon}{\partial x} + \Omega_{xp}\dot{p} + \Omega_{xx}\dot{x} + \Omega_{xt}. \tag{1.18}$$

1.3.2 Density of States Correction

Following these equations, various applications have been made on the electronic properties. For a comprehensive review, see [21]. In this introduction, we emphasis a consequence of these equations, the modified density of states, and provide a general proof in the following. For a general case with time-dependent driven forces, we need to approve that

$$\frac{\partial \sqrt{|M|}}{\partial t} + \frac{\partial \sqrt{|M|}\dot{\xi}_a}{\partial \xi_a} = 0, \tag{1.19}$$

for the dynamical equations,

$$M_{ab}\dot{\xi}_b = \frac{\partial H}{\partial \xi_a} - \Omega_{\xi_a t}, \tag{1.20}$$

where ξ labels x and p, $M = \Omega - J$ is a skew matrix ($M^T = -M$).

Prove: The target Eq. (1.19) can be written as

$$\frac{\partial \dot{\xi}_a}{\partial \xi_a} = -\frac{1}{\sqrt{|M|}}\frac{d\sqrt{|M|}}{dt} = -\frac{1}{2}\frac{1}{|M|}\frac{d|M|}{dt} = -\frac{1}{2}Tr[M^{-1}\frac{dM}{dt}] \tag{1.21}$$

where we have used $\partial|X| = |X|Tr[X^{-1}\partial X]$. Equations of motion Eq. (1.20) can be written as

$$\dot{\xi}_a = (M^{-1})_{ab}(\frac{\partial H}{\partial \xi_b} - \Omega_{\xi_b t}). \tag{1.22}$$

Consider the quantity,

$$\begin{aligned}\frac{\partial\dot{\xi}_a}{\partial\xi_a} &= \frac{\partial(M^{-1})_{ab}}{\partial\xi_a}(\frac{\partial H}{\partial\xi_b}-\Omega_{\xi_b t})+(M^{-1})_{ab}\frac{\partial(\frac{\partial H}{\partial\xi_b}-\Omega_{\xi_b t})}{\partial\xi_a},\\ &= -(M^{-1})_{ab}\frac{\partial M_{bc}}{\partial\xi_a}(M^{-1})_{cd}(\frac{\partial H}{\partial\xi_d}-\Omega_{\xi_d t})-(M^{-1})_{ab}\frac{\partial\Omega_{\xi_b t}}{\partial\xi_a},\\ &= -(M^{-1})_{ab}\frac{\partial M_{bc}}{\partial\xi_a}\dot{\xi}_c-(M^{-1})_{ab}\frac{\partial\Omega_{\xi_b t}}{\partial\xi_a},\end{aligned} \tag{1.23}$$

where we have used $\partial X^{-1}=-X^{-1}\partial X X^{-1}$. Anti-symmetrize the indexes for $\{a,b\}$, and we have

$$A[\frac{\partial M_{bc}}{\partial\xi_a}] = \frac{1}{2}\frac{\partial M_{ba}}{\partial\xi_c}, \tag{1.24}$$

$$A[\frac{\partial\Omega_{\xi_b t}}{\partial\xi_a}] = \frac{1}{2}\frac{\partial\Omega_{\xi_b\xi_a}}{\partial t}. \tag{1.25}$$

Finally we have,

$$\begin{aligned}\frac{\partial\dot{\xi}_a}{\partial\xi_a} &= -\frac{1}{2}(M^{-1})_{ab}\frac{\partial M_{ba}}{\partial\xi_c}\dot{\xi}_c-\frac{1}{2}(M^{-1})_{ab}\frac{\partial M_{ba}}{\partial t}\\ &= -\frac{1}{2}Tr[M^{-1}\frac{dM}{dt}].\end{aligned} \tag{1.26}$$

Eq. (1.19) is proved.

Chapter 2

Electric Field-Induced Effects on Magnetization Dynamics

[1] In this chapter, we provide a semiclassical framework for the dynamics of magnetization implicitly coupled to electronic degrees of freedom, based on the wave-packet method [22]. We found that the Bloch electrons yield a Berry curvature Ω_{mm}, acting as a *magnetic field* in the magnetization space, while the gradient of the electronic free energy with respect to the magnetization acts as a static *electric field* in the magnetization space, in agreement with previous adiabatic theory of magnetization dynamics [20]. These two fields thus govern the dynamics of magnetization as that of Lorentz force to a charged particle. In addition, we identified an extrinsic contribution to the magnetization dynamics, corresponding to the Gilbert damping in the LLG equation, which is not included in the adiabatic theory. A static electric field enters the magnetization equation of motion by modifying the Berry curvature Ω_{mm}, the effective field, and the damping factor as a first-order perturbation.

[1] The contents of this chapter are based on the article: B. Xiong, H. Chen, X. Li and Q. Niu, *Electronic Contribution to the Geometric Dynamics of Magnetization*, Phys. Rev. B. **98**, 035123 (2018). B. Xiong and Q. Niu conceived the research. B. Xiong performed derivation, coding and calculations. B. Xiong and H. Chen wrote the manuscript, which all authors read and commented on.

In particular, the modification to the effective field includes a part proportional to the Berry curvature Ω_{mk} and having a geometric nature. We used a simplified model for the ferromagnet-topological-insulator interface to illustrate the various effects, and showed that the gyromagnetic ratio is renormalized anisotropically and that an in-plane magnetization can be dynamically stable under moderate electric fields.

2.1 Spin-Orbital Torque

Magnetization dynamics is conventionally described by the phenomenological Landau-Lifshitz-Gilbert (LLG) equation [16, 17, 18], in which the effective magnetic field and the damping factor can be associated with various mechanisms such as dipolar interaction, exchange coupling, electron-hole excitations, etc., through microscopic theories [23, 24, 9]. The recently discovered current-induced spin-orbit torques emerge as current-dependent modifications to the LLG equation, and can be consequently categorized as field-like and damping-like torques [25, 9, 26, 27, 28, 2, 4]. In systems with strong spin-orbit coupling and broken inversion symmetry, e.g., GaMnAs, heavy-metal/ferromagnet bilayers and magnetically doped topological insulator heterostructures, magnetization switching using electric current alone through the spin-orbit torque has been achieved experimentally [29, 2, 30, 31, 32, 4]. In antiferromagnets, staggered torques on opposite magnetizations are also generated electrically [33, 34, 35, 4].

Theoretical studies of spin-orbit torques have mostly adopted $s-d$ type

couplings between transport electrons and those contributing to magnetization [25, 9, 26, 27, 2], or a self-consistent-field picture based on the spin density functional theory [28, 36]. Then the spin-orbit torques can be understood as the modification to the effective exchange fields proportional to the current-induced spin densities in inversion symmetry breaking systems, known as the Edelstein effect [37, 9]. However, in general neither the size of the exchange field nor its dependence on order parameter (magnetization) direction is known *a priori* [38, 8, 4]. It is thus more desirable to develop a theoretical framework that does not explicitly depend on the details of the coupling between transport electrons and the magnetization [8, 39].

2.1.1 The Field-like and Anti-damping-like SOT

The spin-orbital torque is originally proposed by Manchon *et al.* in a ferromagnetic two-dimensional electrons gas with Rashba spin-orbital coupling. The inversion symmetry is broken in the sandwich structure of two dissimilar layers, which gives the freedom for a nonzero spin response by external electric fields, $\delta \boldsymbol{s} = \boldsymbol{\chi} \cdot \boldsymbol{E}$. In the presence of electric field, they found that the non-equilibrium electron gives rise to a spin accumulation $\delta \boldsymbol{s}$ [40, 41], which exerts a torque via the exchange interaction on the ferromagnetic order,

$$T = -J_{sd} \delta \boldsymbol{s} \times \boldsymbol{m}, \tag{2.1}$$

where J_{sd} is the exchange constant, and m is the magnetization. The resultant torque is odd on the reversal of magnetization $\boldsymbol{m} \to -\boldsymbol{m}$, and is called the field-like torque.

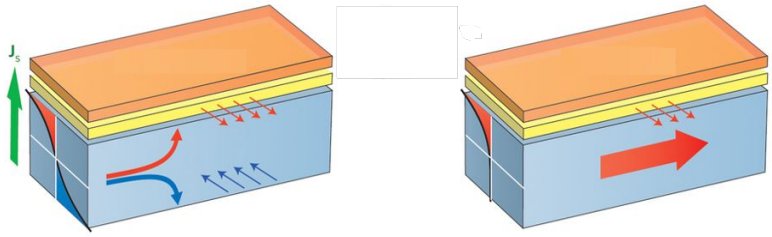

Figure 2.1: (Color online) (Left) SOT is induced by the spin Hall effect and (Right) the Rashba-Edelstein effect in the heavy metal-ferromagnet heterostructures. Adapted from Ref. [1]

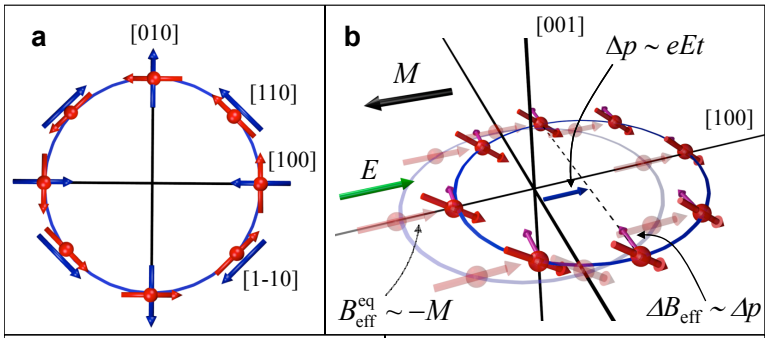

Figure 2.2: (Color online) (a) The Rashba field (red) on electrons of different crystal momentum. (b) The evolution of spin under the field-induced Rashba field. Adapted from Ref. [2]

On the other hand, the spin-orbital torque is introduced in the heterostructures of heavy metals and ferromagnets. With an in-plane electric field, a transverse spin current [42, 43] is generated in the heavy metals and injected into the neighboring ferromagnets. A net spin polarization is then accumulated at the interface, which depends on the magnetization linearly. The resultant torque on the magnetization is thus even under magnetization

reversal,

$$T \sim \boldsymbol{m} \times (\boldsymbol{m} \times \boldsymbol{u}), \tag{2.2}$$

where $\boldsymbol{u}$ is a fixed direction depending on the geometry of the setup. This type of SOT is called the (anti-)damping-like SOT.

The Berry curvature mechanism for SOT is proposed by H. Kurebayashi *et al.*[2] In GaMnAs, a ferromagnetic semiconductor, they found an intrinsic contribution to the field-induced spin (torques), besides the contribution from the non-equilibrium electrons found by Manchon *et al.* The field-induced spin is obtained by considering the carrier spin evolution under effective magnetic fields. Due to the spin-orbital coupling $H_R = \alpha s \times p \cdot \hat{z}$, the effective magnetic fields acquire a component proportional to $p \times \hat{z}$. The electric field enters by accelerating the electrons $\dot{p} = -eE$, thus generating an extra effective magnetic field, $\Delta B_{eff} \sim \Delta p$, in Fig. 2.2. The field-induced spin depends linearly on the magnetization, resulting in an anti-damping-like torque. Different from the spin Hall mechanism, the spin accumulation is produced in the semiconductor without external injection. It is an intrinsic property of the electronic band structures. In comparison, the non-equilibrium contribution relies on the relation time and is thus extrinsic.

2.2 Semiclassical Formulation

The following sections introduce the semiclassical magnetization dynamics for uniform materials. The magnetization is regarded as an *external* order parameter that couples with the electronic system. In the end, we obtain

a theory of magnetization dynamics in the presence of an electric field, where the SOT and other effects are found.

2.2.1 Coupled Dynamics of Electrons and Magnetization

We start from a general Hamiltonian of Bloch electrons implicitly depending on the order parameter $\boldsymbol{m}$, $\hat{H}_e(\boldsymbol{q};\boldsymbol{m})$, where $\boldsymbol{q}$ is the crystal momentum. External electromagnetic fields are described by the scalar and vector potentials $(\phi, \boldsymbol{A})$ that enter the Hamiltonian through minimum coupling ($\hbar = 1$, $e = |e|$),

$$\hat{H} = \hat{H}_e(\boldsymbol{q} + e\boldsymbol{A};\boldsymbol{m}) - e\phi. \tag{2.3}$$

Following Ref. [12], a wave packet is constructed with center position $\boldsymbol{x}$ and center physical momentum $\boldsymbol{k}$ from the Bloch eigenstates of the local electronic Hamiltonian. The Lagrangian of a single wave packet reads as

$$\mathcal{L} = \dot{\boldsymbol{x}} \cdot [\boldsymbol{k} - e\boldsymbol{A}(\boldsymbol{x},t)] + \dot{\boldsymbol{k}} \cdot \boldsymbol{A}_{\boldsymbol{k}} + \dot{\boldsymbol{m}} \cdot \boldsymbol{A}_{\boldsymbol{m}} - [\varepsilon - e\phi(\boldsymbol{x},t)], \tag{2.4}$$

with $\boldsymbol{A}_{\boldsymbol{\lambda}} = i\langle u|\nabla_{\boldsymbol{\lambda}} u\rangle$ ($\lambda = \boldsymbol{k}$ or $\boldsymbol{m}$) the Berry connections of the Bloch state $|u\rangle$, and ε the wave packet energy. For notational simplicity we have dropped the band index. The Lagrangian depends on $(\boldsymbol{x}, \boldsymbol{k})$ of the wave packets and magnetization $\boldsymbol{m}$. Thus a set of coupled equations of motion for all three variables can be derived from the Lagrangian principle [21]:

$$\dot{\boldsymbol{k}} = -e\boldsymbol{E}, \tag{2.5}$$

$$\dot{\boldsymbol{x}} = \frac{\partial \varepsilon}{\partial \boldsymbol{k}} + \dot{\boldsymbol{k}} \cdot \Omega_{\boldsymbol{kk}} + \dot{\boldsymbol{m}} \cdot \Omega_{\boldsymbol{mk}}, \tag{2.6}$$

$$\int [d\boldsymbol{k}] f \left(\dot{\boldsymbol{m}} \cdot \Omega_{\boldsymbol{mm}} + \dot{\boldsymbol{k}} \cdot \Omega_{\boldsymbol{km}} + \frac{\partial \varepsilon}{\partial \boldsymbol{m}} \right) = 0, \tag{2.7}$$

where the Berry curvatures $\Omega_{\lambda_i\lambda_j} = -2\mathrm{Im}\langle\partial u/\partial\lambda_i|\partial u/\partial\lambda_j\rangle$, $\boldsymbol{\lambda} = \boldsymbol{k}$ or $\boldsymbol{m}$. Eq. (2.7) is obtained by summing over all occupied states, and f is the distribution function for the electrons. Note the magnetization dynamics enters the electron equations of motion through $\Omega_{\boldsymbol{mk}}$ in Eq. (2.6), i.e., the charge pumping effects [21]. The terms in the square brackets of Eq. (2.7) can be viewed as conjugates of the right hand side of Eq. (2.6), by interchanging $\boldsymbol{k}$ and $\boldsymbol{m}$. This is a manifestation of the reciprocity between charge pumping due to magnetization precession and electric-current-induced spin-orbit torque.

The nonequilibrium response of the electrons to an external electric field and/or a dynamical $\boldsymbol{m}$ is accounted for using the semiclassical Boltzmann equation, according to which the deviation of the distribution function from the equilibrium Fermi-Dirac distribution $f_0[\varepsilon(\boldsymbol{k},\boldsymbol{m})]$ is

$$\delta f = -\tau\frac{\partial f_0}{\partial\varepsilon}\left(\dot{\boldsymbol{k}}\cdot\frac{\partial\varepsilon}{\partial\boldsymbol{k}} + \dot{\boldsymbol{m}}\cdot\frac{\partial\varepsilon}{\partial\boldsymbol{m}}\right), \tag{2.8}$$

where we have assumed a grand canonical ensemble with fixed temperature and chemical potential. τ is the relaxation time which we take as a constant for simplicity. Generalization to including more specific scattering mechanisms is straightforward but involved, and does not necessarily provide additional insight on the main issues considered in this work.

The equations (2.5-2.8) complete our semiclassical description of coupled magnetization and electron dynamics in the presence of external electric fields, though they can be easily extended to including magnetic fields and other perturbations.

In the absence of electric fields, $\dot{\boldsymbol{k}} = 0$, and we can obtain from Eq. (2.8) and Eq. (2.7) the following equations of motion of the magnetization,

$$\dot{\boldsymbol{m}} \cdot (\bar{\Omega}_{\boldsymbol{mm}} + \eta_{\boldsymbol{mm}}) - \boldsymbol{H} = 0, \tag{2.9}$$

in getting which we have ignored higher order $\dot{\boldsymbol{m}}^2$ terms by assuming that the magnetization dynamics is slow compared to typical electronic time scales. The Berry curvature $\bar{\Omega}$, the damping coefficient η and the effective field $\boldsymbol{H}$ in the equation above are respectively

$$\bar{\Omega}_{\boldsymbol{mm}} = \int [d\boldsymbol{k}] f_0 \Omega_{\boldsymbol{mm}}, \tag{2.10}$$

$$\eta_{\boldsymbol{mm}} = -\tau \int [d\boldsymbol{k}] \frac{\partial f_0}{\partial \varepsilon} \frac{\partial \varepsilon}{\partial \boldsymbol{m}} \frac{\partial \varepsilon}{\partial \boldsymbol{m}}, \tag{2.11}$$

$$\boldsymbol{H} = -\frac{\partial G}{\partial \boldsymbol{m}}, \tag{2.12}$$

where G is the free energy of the electron system. For non-interacting electrons $G = -\beta^{-1} \int [d\boldsymbol{k}] \ln[1 + e^{-\beta(\varepsilon - \mu)}]$ for a single band, where $\beta = 1/k_B T$. Interaction effects may be included in G through different levels of approximations, which will also modify the way magnetization appears in G. At this point we will leave G as a general electron free energy depending on $\boldsymbol{m}$ implicitly.

According to Eq. (2.9), the static magnetization configuration is where effective field vanishes, $H|_{\boldsymbol{m}=\boldsymbol{m}_0} = 0$. The frequency of magnetization motion around $\boldsymbol{m}_0$ is determined by the $\bar{\Omega}_{\boldsymbol{mm}}$ and $\boldsymbol{H}$ terms, with typical frequency $\omega \sim GHz$. The typical relaxation time of electronic excitations is $\tau \sim ps$. Hence the damping term is smaller compared with $\bar{\Omega}_{\boldsymbol{mm}}$ and $\boldsymbol{H}$ terms. The

ignored $\dot{\boldsymbol{m}}^2$ term in Eq. (2.9) is

$$\dot{\boldsymbol{m}} \cdot \int [d\boldsymbol{k}] \Omega_{\boldsymbol{mm}} (\dot{\boldsymbol{m}} \cdot \frac{\partial \varepsilon}{\partial \boldsymbol{m}})(-\tau \frac{\partial f_0}{\partial \varepsilon}), \tag{2.13}$$

which is smaller than the damping terms. Essentially we assume the magnitude of quantities are in the following order,

$$\int [d\boldsymbol{k}] \Omega_{\boldsymbol{mm}} (\dot{\boldsymbol{m}} \cdot \frac{\partial \varepsilon}{\partial \boldsymbol{m}})(-\tau \frac{\partial f_0}{\partial \varepsilon}) \ll -\tau \int [d\boldsymbol{k}] \frac{\partial f_0}{\partial \varepsilon} \frac{\partial \varepsilon}{\partial \boldsymbol{m}} \frac{\partial \varepsilon}{\partial \boldsymbol{m}} \ll \int [d\boldsymbol{k}] f_0 \Omega_{\boldsymbol{mm}}. \tag{2.14}$$

We only consider the transverse modes ($\dot{\boldsymbol{m}}$ perpendicular to $\boldsymbol{m}$) of the magnetization dynamics in this work, although Eq. (2.9) can be used for the longitudinal mode as well. The magnetization is thus described by the polar angle θ and the azimuthal angle ϕ. Eq. (2.9) can then be converted to the familiar form of the LLG equation,

$$\dot{\boldsymbol{m}} = -\gamma \boldsymbol{m} \times (\boldsymbol{H} - \eta_{\boldsymbol{mm}} \cdot \dot{\boldsymbol{m}}), \tag{2.15}$$

where the gyromagnetic ratio γ is related to the Berry curvature through

$$\bar{\boldsymbol{\Omega}} = \boldsymbol{m}/\gamma m^2, \tag{2.16}$$

where $\bar{\Omega}_i = \varepsilon_{ijk} \bar{\Omega}_{jk}/2$ is the vector form of the Berry curvature tensor, which is along the radial direction for transverse modes thus leading to the above form. Expressions similar to Eq. (2.9), but *without the damping term*, have been derived using the adiabatic theory [19]. Since the damping term is explicitly dependent on the relaxation time, which is ultimately due to dissipative microscopic processes such as electron-phonon scattering and electron-impurity

scattering, we call it extrinsic contribution to the magnetization dynamics. Note Eq. (2.11) suggests η is positive definite, which means it always leads to energy dissipation through Eq. (2.15). The relaxation time approximation here can be further developed by including the microscopic scattering mechanism within the Boltzmann equation framework [44], which is not the focus of this work.

The remaining terms are intrinsic contributions from the electron degrees of freedom. In particular, from Eq. (2.9) one can see that the two intrinsic terms are formally similar to the Lorentz force of a charged particle, with the antisymmetric part of $\Omega_{\boldsymbol{mm}}$ (or equivalently the vector form $\boldsymbol{\Omega_m}$) analogous to the magnetic field and $\boldsymbol{H}$ playing the role of the electric field.

2.2.2 Electric Field-Induced Correction of LLG

Electric fields enter our formalism through the equation of motion for $\boldsymbol{k}$ [Eq. (2.5)], which makes the 2nd term in the integrand of Eq. (2.7) nonzero and also contributes to the nonequilibrium distribution function δf in Eq. (2.8). After some algebra, we arrive at the same equation as Eq. (2.9), but with $\boldsymbol{H}$, $\bar{\Omega}_{\boldsymbol{mm}}$, and $\eta_{\boldsymbol{mm}}$ acquiring the following corrections proportional to the electric field:

$$\boldsymbol{H}^E = e\boldsymbol{E}\cdot\int[d\boldsymbol{k}]\left(\Omega_{\boldsymbol{km}}f_0 - \tau\frac{\partial\varepsilon}{\partial\boldsymbol{k}}\frac{\partial\varepsilon}{\partial\boldsymbol{m}}\frac{\partial f_0}{\partial\varepsilon}\right), \tag{2.17}$$

$$\bar{\Omega}^E_{m_im_j} = e\tau\boldsymbol{E}\cdot\int[d\boldsymbol{k}]\left[\frac{\partial\varepsilon}{\partial\boldsymbol{k}}\Omega_{m_im_j} - \left(\Omega_{\boldsymbol{k}m_i}\frac{\partial\varepsilon}{\partial m_j}\right)_{\mathrm{A}}\right]\frac{\partial f_0}{\partial\varepsilon}, \tag{2.18}$$

$$\eta^E_{m_im_j} = e\tau\boldsymbol{E}\cdot\int[d\boldsymbol{k}]\left(\Omega_{\boldsymbol{k}m_i}\frac{\partial\varepsilon}{\partial m_j}\right)_{\mathrm{S}}\frac{\partial f_0}{\partial\varepsilon} \tag{2.19}$$

where subscript S (A) means the part of $\Omega_{\boldsymbol{k}m_i}\frac{\partial\varepsilon}{\partial m_j}$ that is symmetric (antisymmetric) under $i \leftrightarrow j$. We next discuss the physical meanings of these results in detail.

For the correction to the effective field, $\boldsymbol{H}^E$, the first term in Eq. (2.17) has a geometric nature and is an intrinsic contribution from the Fermi sea electrons. It is of $\Omega_{\boldsymbol{m}t}$ type, where the time variation is due to the momentum change of a single wave packet driven by $\boldsymbol{E}$: $\partial_t = \dot{\boldsymbol{k}}\cdot\partial_{\boldsymbol{k}} = -e\boldsymbol{E}\cdot\partial_{\boldsymbol{k}}$. We note there is a nice identity connecting $\Omega_{\boldsymbol{m}t}$ and the *magnetic field* in magnetization space $\boldsymbol{\Omega}_{\boldsymbol{m}}$:

$$\partial_t\boldsymbol{\Omega}_m + \nabla_{\boldsymbol{m}}\times\Omega_{\boldsymbol{m}t} = 0. \tag{2.20}$$

Since $\Omega_{\boldsymbol{m}t} = \Omega_{\boldsymbol{m}\boldsymbol{k}}\cdot(-e\boldsymbol{E})$ is a correction to the static effective *electric field* $\boldsymbol{H}$ (Eq. 2.12) in the magnetization space, above equation is a magnetic analog of the Faraday's law for charged particles. The 2nd term in Eq. (2.17) is extrinsic since it is proportional to τ, and does not have an electromagnetism analog.

We now move on to $\bar{\Omega}^E_{\boldsymbol{m}\boldsymbol{m}}$ and $\eta^E_{\boldsymbol{m}\boldsymbol{m}}$, which are all Fermi surface contributions due to the non-equilibrium part of the distribution function δf. They are important in magnetic metals [45] and should be discussed on an equal footing as $\boldsymbol{H}^E$ for current-induced effects on magnetization dynamics. In the form of Eq. (2.15), $\bar{\Omega}^E_{\boldsymbol{m}\boldsymbol{m}}$ renormalizes the gyromagnetic ratio as $\gamma' = \gamma/(1+\gamma/\gamma^E)$, where $\gamma^E \equiv (\boldsymbol{m}\cdot\bar{\boldsymbol{\Omega}}^E)^{-1}$, while $\eta^E_{\boldsymbol{m}\boldsymbol{m}}$ modifies the damping tensor as $\eta' = \eta+\eta^E$.

It is interesting to note that η^E does not have to be positive definite. A negative definite total damping will make the free energy minima dynami-

cally unstable while the maxima dynamically stable. Thus in addition to the potential of switching the magnetization between different easy directions, a suitably chosen electric field can in principle switch the magnetization between easy and hard directions, which provides a new mechanism (though volatile) for current driven reading and writing processes in magnetic memory devices.

$\boldsymbol{H}^E$ also provides new insights on the charge pumping effect of a nonzero $\dot{\boldsymbol{m}}$ [11, 46]. It is heuristic to compare Eq. (2.17) with the expression of the total current driven by the magnetization motion $\dot{\boldsymbol{m}}$,

$$\begin{aligned} \boldsymbol{j}_t &= e\int [d\boldsymbol{k}] \left(\Omega_{\boldsymbol{km}} f_0 + \tau \frac{\partial \varepsilon}{\partial \boldsymbol{k}} \frac{\partial \varepsilon}{\partial \boldsymbol{m}} \frac{\partial f_0}{\partial \varepsilon} \right) \cdot \dot{\boldsymbol{m}} \\ &= \boldsymbol{j}_i + \boldsymbol{j}_e, \end{aligned} \tag{2.21}$$

which consists of the pumping current $\boldsymbol{j}_i$ and relaxation related current $\boldsymbol{j}_e$, where the subscript i and e means intrinsic and extrinsic contribution, respectively. The current expression is kept to the first order in $\dot{\boldsymbol{m}}$ considering slow magnetization motion. Since $P \equiv \boldsymbol{H}^E \cdot \dot{\boldsymbol{m}}$ has the meaning of power density on the magnetization freedom, it is inductive to consider the energy conversion from the electric power on current, $\boldsymbol{j} \cdot \boldsymbol{E}$, to magnetic energy density G, which is

$$\frac{dG}{dt} = \boldsymbol{j}_i \cdot \boldsymbol{E} - \boldsymbol{j}_e \cdot \boldsymbol{E}. \tag{2.22}$$

The electric power on the intrinsic current contributes to increase the magnetic energy, while the power on extrinsic current tends to decrease the magnetic energy. This is because the intrinsic current respects the time reversal symmetry, while the extrinsic current breaks the time reversal symmetry. Indeed,

according the Onsager relation,

$$\boldsymbol{j}_i(\boldsymbol{m}) = -\boldsymbol{j}_i(-\boldsymbol{m}), \tag{2.23}$$

$$\boldsymbol{j}_e(\boldsymbol{m}) = \boldsymbol{j}_i(\boldsymbol{m}). \tag{2.24}$$

where, the intrinsic and extrinsic part of the effective field, $\boldsymbol{H}_i^E$ and $\boldsymbol{H}_e^E$, are odd and even, respectively, under time reverse operation, $\boldsymbol{m} \to -\boldsymbol{m}$. The corresponding torques, $\tau_{so} = -\gamma \boldsymbol{m} \times \boldsymbol{H}^E$, are categorized as damping-like and field-like torques.

For insulators, the extrinsic part of the effective fields vanishes and only the intrinsic one contributes. The change of the polarization density ("pumping") after $\boldsymbol{m}$ completes a closed path in its configuration space is obtained by integrating $\boldsymbol{j}_i$ over this period. A finite charge pumping thus corresponds to a nonzero work density, and is related to the curl of $\boldsymbol{H}_i^E$ in the magnetization space through

$$\begin{aligned} W = \oint \boldsymbol{j}_i \cdot \boldsymbol{E} dt = \oint \boldsymbol{H}_i^E \cdot d\boldsymbol{m} \\ = \iint \nabla_{\boldsymbol{m}} \times \boldsymbol{H}_i^E \cdot d\boldsymbol{\sigma}_{\boldsymbol{m}}, \end{aligned} \tag{2.25}$$

where we have used the Stokes theorem, and $d\boldsymbol{\sigma}_{\boldsymbol{m}}$ is the infinitesimal area in the magnetization space. Thus with finite charge pumping along any close curve on the magnetization sphere, $\boldsymbol{H}_i^E$ must not be conservative, i.e., it cannot be written as a gradient of certain scalar free energy. If the electronic system is gapped along a close curve l on the magnetization sphere, the charge pumped in one circle is quantized in proper units, and the same for the work density

W. Since the quantized quantity changes in a discretized way and the curve l can be continuous varying, nonzero charge pumping implies singular points on the magnetization sphere, which are the energy degenerate points with energy gap closed. When the curve l passes the singular points, the work density W along the curve changes by some integer units.

Since the electric field enters our formalism only through its modification on momentum [Eq. (3)], our theory can be straightforwardly generalized to other time-varying perturbations that influence wave-packet dynamics in similar ways, which will give both Fermi-surface contributions and Fermi-sea contributions through the Berry curvature $\Omega_{\boldsymbol{m}t}$. For example, a potential application is the magnetization dynamics driven by sound wave [47, 48]. Separately, our formalism can be applied to the slow dynamics of other order parameters in crystalline solids, and to its dependence on electromagnetic fields through the electron degrees of freedom.

Before ending this section, we translate our results Eq. (2.17-2.19) into the commonly used spin-orbit torque language. For small electric fields they can be converted to additional terms added to the right hand side of the LLG equation Eq. (2.15):

$$\dot{\boldsymbol{m}} = -\gamma \boldsymbol{m} \times (\boldsymbol{H} - \eta_{\boldsymbol{mm}} \cdot \dot{\boldsymbol{m}}) - \gamma \boldsymbol{\tau}_{so}, \tag{2.26}$$

where $\boldsymbol{\tau}_{so} = \boldsymbol{\tau}_{so}^{H} + \boldsymbol{\tau}_{so}^{\gamma} + \boldsymbol{\tau}_{so}^{\eta}$ with the separate terms being

$$\boldsymbol{\tau}_{so}^{H} = \boldsymbol{m} \times \boldsymbol{H}^{E}, \tag{2.27}$$

$$\boldsymbol{\tau}_{so}^{\gamma} = -\gamma/\gamma^{E}\boldsymbol{m} \times (\boldsymbol{H} + \eta\gamma\boldsymbol{m} \times \boldsymbol{H}), \tag{2.28}$$

$$\boldsymbol{\tau}_{so}^{\eta} = \gamma\eta^{E}\boldsymbol{m} \times (\boldsymbol{m} \times \boldsymbol{H}). \tag{2.29}$$

For the special $s-d$ type coupling, H^{E} is proportional to the spin density response to electric fields since $\partial\hat{H}/\partial\boldsymbol{m} \sim \boldsymbol{s}$, in agreement with previous studies [37, 30, 9, 28], though our formalism is not limited to this coupling form. Morever, there are additional torques $\boldsymbol{\tau}_{so}^{\gamma}$ and $\boldsymbol{\tau}_{so}^{\eta}$ that cannot be directly explained using spin density response to electric fields. They can, however, always be classified into either field-like or damping-like torques depending on whether there is a sign change upon $\boldsymbol{m} \to -\boldsymbol{m}$.

2.3 3D Topological Insulator-Ferromagnets Interface

As a concrete example, we consider a 2D toy model that can be used to describe the interface between a ferromagnetic insulator and a 3D topological insulator (TI) [10, 49, 50, 51, 52, 53]:

$$\hat{H}(\boldsymbol{m}) = \hbar v(-k_y\sigma_x + k_x\sigma_y) + J\boldsymbol{m} \cdot \boldsymbol{\sigma}, \tag{2.30}$$

where $\boldsymbol{m}$ is the 2D magnetization of the ferromagnet, $\boldsymbol{\sigma}$ is the Pauli matrix vector for the spin operators, v is the Fermi velocity of the Dirac surface electrons of the TI, and J is the exchange coupling strength between $\boldsymbol{m}$ and $\boldsymbol{\sigma}$. Bulk and Rashba surface states are ignored for simplicity [54, 46]. The

exchange coupling opens a gap proportional to the z component of $\boldsymbol{m}$. We consider zero temperature and set the chemical potential $\mu = 0$. The Berry curvature of the lower band is calculated similarly as the $\vec{k} \cdot \vec{\sigma}$ model [21]

$$\bar{\Omega}^s_{\theta\phi} = \frac{\alpha^2 |\sin 2\theta|}{8\pi a^2} \mathrm{sgn}(\alpha), \tag{2.31}$$

where $\alpha = Jma/\hbar v$ is the exchange energy measured in typical scales of the kinetic energy $\epsilon_0 = \hbar v/a$ (a is the lattice constant). Using relation Eq. (2.16), the Berry curvature gives an anisotropic gyromagnetic ratio

$$\gamma_s(\theta) = \frac{4\pi m a^2}{\hbar \alpha^2 |\cos\theta|} \mathrm{sgn}(\alpha). \tag{2.32}$$

We should note that the ferromagnet by itself has a gyromagnetic ratio, denoted as γ_f, and the overall gyromagnetic ratio γ is corrected as

$$\gamma^{-1} = {\gamma_f}^{-1} + {\gamma_s}^{-1}, \tag{2.33}$$

or equivalently

$$\gamma = \gamma_f \cdot \frac{1}{1 + \gamma_f/\gamma_s(\theta)}. \tag{2.34}$$

The variation of γ as $\boldsymbol{m}$ moving across the magnetization sphere is shown in Fig. 2.8(a). On the equator ($\theta = \pi/2$), $\gamma = \gamma_f$; at the north and south poles, $\gamma = \gamma_f/(1 + \gamma_f \hbar\alpha^2/4\pi m a^2 \mathrm{sgn}(\alpha))$. This angular dependence of gyromagnetic ratio should be able to be detected by ferromagnetic resonance experiments in such systems.

The free energy density at zero temperature is calculated by integrating the energy of the lower bands. Ignoring a constant term, we get

$$G^s = -J_0 m_z^2 \tag{2.35}$$

where $J_0 = \epsilon_0 k_c \alpha^2 / 4\pi m^2 a$ and k_c is the momentum cutoff. G^s has two minima at the north and south poles, as shown in Fig. 2.8(b). Thus the surface states provide a perpendicular magnetic anisotropy for the ferromagnet. For simplicity we ignored the magnetic anisotropy energy of the ferromagnet itself. For $m_z \neq 0$, there is no contribution from the surface state electrons to η because of the finite gap, and if the intrinsic damping of the ferromagnet is ignorable the magnetization should move along equal-energy lines without driving forces, along the directions determined by $-\gamma \boldsymbol{m} \times \boldsymbol{H}$ [Eq. (2.15)], as illustrated in Fig. 2.8(b).

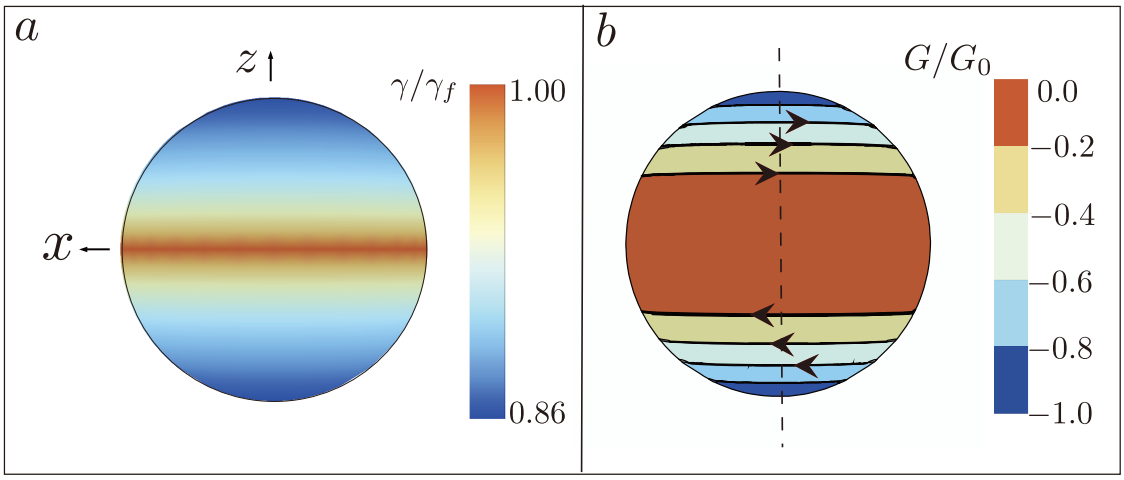

Figure 2.3: (Color online) (a) Renormalized gyromagnetic ratio γ and (b) Contour plot of free energy G^s via coupling to the topological surface states. The arrows indicate the directions of magnetization motion. Parameters: $\gamma_f = 2ma^2/\hbar, \alpha = 1$

We now consider the effect of an electric field along x direction on the magnetization dynamics. For nonzero m_z all Fermi surface contributions in

Eqs. (2.17-2.19) are zero, and the only finite term is the Fermi sea contribution in $\boldsymbol{H}^E$:

$$\boldsymbol{H}^E = -\frac{eE|\alpha|}{4\pi ma}\mathrm{sgn}(m_z)\hat{x}. \tag{2.36}$$

The magnetoelectric effect originates from the strong spin-orbital coupling in TI [55, 56, 10, 46]. It has constant magnitude but opposite directions depending on the sign of m_z. The curl of $\boldsymbol{H}^E$ is thus zero everywhere except on the equator, which also means nonzero charge is pumped by magnetization dynamics when the precession axis is in plane [57]. Based on our discussion in the previous section we can only define free energy functions separately for the north (N) and the south (S) hemispheres as G_N and G_S but not globally:

$$G_N = -J_0 m_z^2 + \frac{eE|\alpha|}{4\pi ma}m_x, \tag{2.37a}$$

$$G_S = -J_0 m_z^2 - \frac{eE|\alpha|}{4\pi ma}m_x. \tag{2.37b}$$

On each hemisphere, the 2nd term in the free energy implies a magnetization-dependent polarization, which will be interesting to detect experimentally. Moreover, since $G_N - G_S \propto m_x$, they cannot be connected by a constant energy shift across the equator. The electric field thus shifts the two free energy minima at the north and the south poles in opposite directions, and distorts the equal energy lines in the vertical direction, as shown in Fig. 2.4. In addition, the opposite signs of G_N and G_S very close to the equator make half of the equator dynamically stable, as can be seen from the arrows pointing to the equator from both above and below in Fig. 2.4. Specifically, if we still assume a vanishing intrinsic damping of the ferromagnet, when the magnetization is very

close to the equator with $\phi \in (\pi, 2\pi)$, or more generally when it is between the two critical trajectories determined by $G_{N/S} = -eE|\alpha|/4\pi a$, it will follow the equal energy lines and end up on the half equator with $\phi \in (0, \pi)$. Conversely, for a magnetization outside of the region between the two critical trajectories, i.e., $G_{N/S} < -eE|\alpha|/4\pi a$, it will keep precessing around one of the free energy minima. When there is a small damping, the size of the attraction area around the half equator reduces because energy is dissipated during evolution.

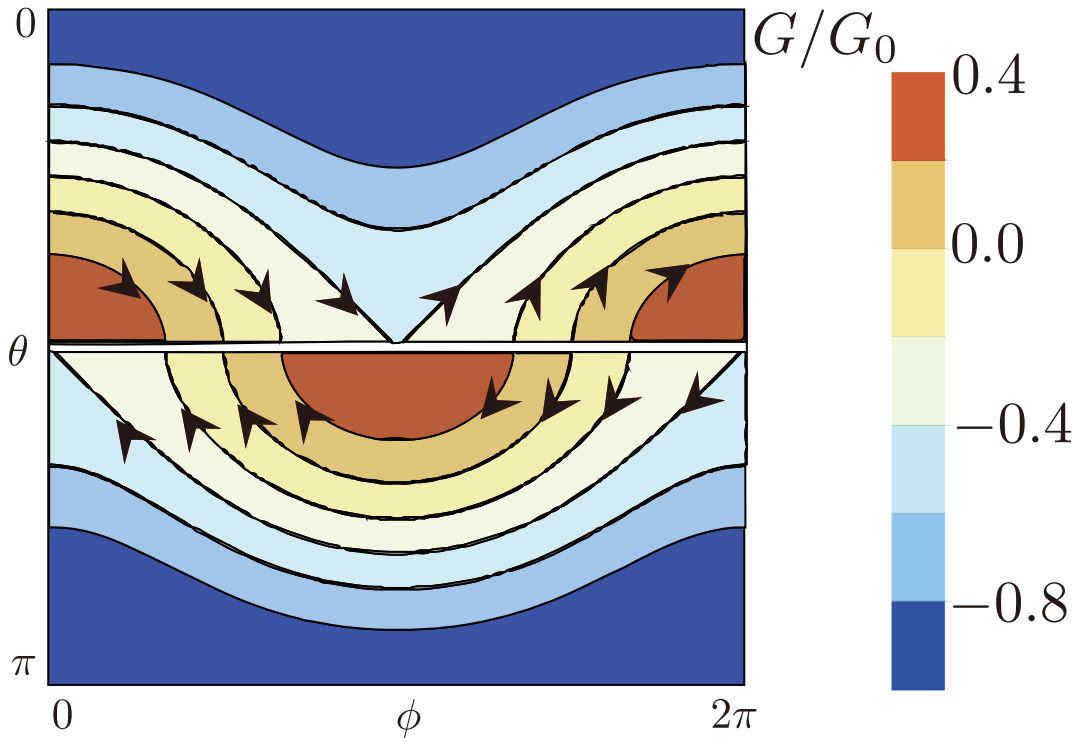

Figure 2.4: (Color online) Contour plot of free energies G_N and G_S in the presence of electric field. Parameters: $\gamma_f = 2ma^2/\hbar, \alpha = 1$, $eE|\alpha|/4\pi J_0 m^2 a = 0.4$.

In the limiting case of strong electric fields $eE|\alpha|/4\pi a > 2J_0m^2$, the critical trajectories disappear on the magnetization sphere and the magnetization will always evolve to the stable half equator. Since without the magnetic field the magnetization has a perpendicular anisotropy due to the topological surface states, electric fields can lead to dynamical switching between easy (out-of-plane) and hard (in-plane) directions. This mechanism is unique to the FM/TI system and is independent of the easy-hard-axes switching due to a negative-definite damping tensor discussed in the last section.

2.4 2D Topological Insulator-Ferromagnets Interface

In the above example, the Dirac point of 2D Dirac electrons is shift in the momentum space by an amount linear to the x and y components of magnetization. The z component opens the energy gap everywhere on the magnetization sphere except on the equator, forming a singular line that separates the northern and southern hemisphere. As a result, a globally well-defined free energy can not be found to describe the effective field. The free energy instead has to be defined separately on each hemisphere, and changes discontinuous across the equator.

Now we consider that a 2D topological insulator is attached with a 1D ferromagnet. The low-energy effective Hamiltonian of electrons is

$$\hat{H}(\boldsymbol{m}) = \hbar v k \sigma_y + J\boldsymbol{m}\cdot\boldsymbol{\sigma}, \tag{2.38}$$

where v is the Fermi velocity and J is the coupling constant. The Dirac point

is shift to k_D by the y component of magnetization with $\hbar v k_D + J m_y = 0$. (We assume that the momentum shift is always within the Brillouin zone.) The energy gap of Dirac electrons is still closed only when the magnetization components m_x and m_z are zero. Hence there are two singular points on the magnetization sphere along the y direction with $m_y = \pm m$. Because the magnetization space has rotational symmetry around the y axis (not z axis), the magnetization is parametrized with polar angle θ with respect to the y axis, and azimuthal angle ϕ from the z axis to the x axis, $(m_x, m_y, m_z) = m(\sin\theta\sin\phi, \cos\theta, \sin\theta\cos\phi)$. We assume that temperature is zero and that the chemical potential is in the gap (hence the lower band is fully filled and the upper band is empty). With these setups, we derive the Berry curvature in magnetization space as,

$$\Omega_{\theta\phi} = \frac{\alpha \sin\theta}{2\pi a}, \tag{2.39}$$

where $\alpha = Jma/\hbar v$ is the ratio between the exchange energy Jm and the kinetic energy scale $\hbar v/a$, a is the lattice constant. The Berry curvature gives the gyromagnetic ratio from the Dirac electrons $\gamma_s = m\sin\theta/\hbar\Omega_{\theta\phi} = 2\pi ma/\alpha\hbar$. On the other hand, the 1D ferromagnet itself has the gyromagnetic ratio $\gamma_f = 2ma/\hbar$, with the assumption of spin contribution to magnetization. Putting together, the gyromagnetic ratio of the 1D ferromagnet is normalized as the following,

$$\gamma = \gamma_f \frac{1}{1 + \gamma_f/\gamma_s} = \gamma_f \frac{1}{1 + \alpha/\pi}. \tag{2.40}$$

When $\alpha \to 0$, the gyromagnetic ratio reverts to γ_f as expected. The renormalization effect is uniform on the magnetization sphere, even though the y

axis is not equivalent to x or z axis.

When an electric field is applied along the direction of the 1D ferromagnet, the induced field $\boldsymbol{H}$ is calculated with only the intrinsic contribution included,

$$\boldsymbol{H}^E = \frac{eE}{2\pi m}\frac{-\vec{e}_\phi}{\sin\theta}. \tag{2.41}$$

where projection of the induced field on the sphere has been made. The field tends to rotate the magnetization along the $-y$ axis. It is uniform in the azimuthal angle ϕ, reflecting the rotational symmetry of magnetization around the y axis. However, the field varies in θ, and diverges close to the singular points. Note the divergent factor $1/\sin\theta$ is inversely proportional to the perimeter of the circle on the magnetization sphere of constant θ, which leads to the following topological argument: As magnetization moves on a close line, the work density from the electric field on the electronic system is an invariant,

$$\oint \boldsymbol{H}^E \cdot d\boldsymbol{m} = eEC. \tag{2.42}$$

The integer C is determined by the number of circles that the magnetization goes around the y axis, with positive direction corresponding to the angular velocity in the $-y$ direction. Note the path of magnetization should avoid the singular points at $m_y = \pm m$ (where external contribution becomes important). Because the work density depends on the history of magnetization path, it prevents the definition of a global free energy G so that $\boldsymbol{H}^E = -\partial G/\partial \boldsymbol{m}$. Instead, a line cut should be made from the north pole to the south pole, and local free energies can be defined piece-wisely on each area.

The quantized work density is topological in the sense that: It does not depend on the details of the path, or the speed of magnetization motion on the path. The topological relation can also be appreciated from the current pumping point of view. When the magnetization goes around the y axis in an adiabatic way, a quantized amount of charge is pumped, which gives the quantized power density eE/a; if the path of magnetization does not enclose the singular points at $m_y = \pm m$, zero charge is pumped and the power density vanishes over this period. This adiabatic charge pumping is topological, and does not depend on the details of the path.

2.4.1 Evolution on the Magnetization Sphere

In 1D magnetic materials, the magnetization tends to align within the material, represented by an easy axis with the anisotropic energy $\varepsilon_{uni} = -K_{uni}\hat{m}_x^2 = -K_{uni}\sin^2\theta\sin^2\phi$. The equilibrium positions are at $\phi_f = \pi/2, 3\pi/2$, Fig. 2.5. (The electromagnetic energy of the magnetization is lower.)

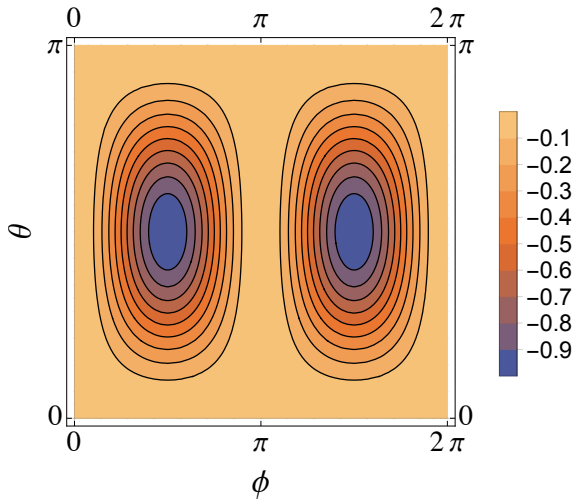

Figure 2.5: (Color online) The energy contour of 1D ferromagnets with easy axis along x direction.

Without damping, the magnetization goes around x axis on the magnetization sphere. With damping, the magnetization evolves to the points of lowest energy on the x axis, Fig. 2.6. The Gilbert damping is taken into account with diagonal elements in the damping matrix, $\alpha_{\theta\theta} = 2\alpha$, $\alpha_{\phi\phi} = 2\alpha \sin^2\theta$. The equation of motion for the magnetization is,

$$\begin{pmatrix} 2\alpha & -A\sin\theta \\ A\sin\theta & 2\alpha\sin^2\theta \end{pmatrix} \begin{pmatrix} \dot{\theta} \\ \dot{\phi} \end{pmatrix} = \begin{pmatrix} -\partial\varepsilon_{uni}/\partial\theta \\ -\partial\varepsilon_{uni}/\partial\phi \end{pmatrix}. \tag{2.43}$$

where $A = \hbar/2a$ (Berry curvature density $\times$ $\hbar$). The equilibrium state ϕ_f depends on the initial condition ϕ_i: $\phi_f = \pi/2$ if $\phi_i \in (0, \pi)$, and $\phi_f = 3\pi/2$ if $\phi_i \in (\pi, 2\pi)$. The continental divider between the two cases is the y-z plane, Fig. 2.6.

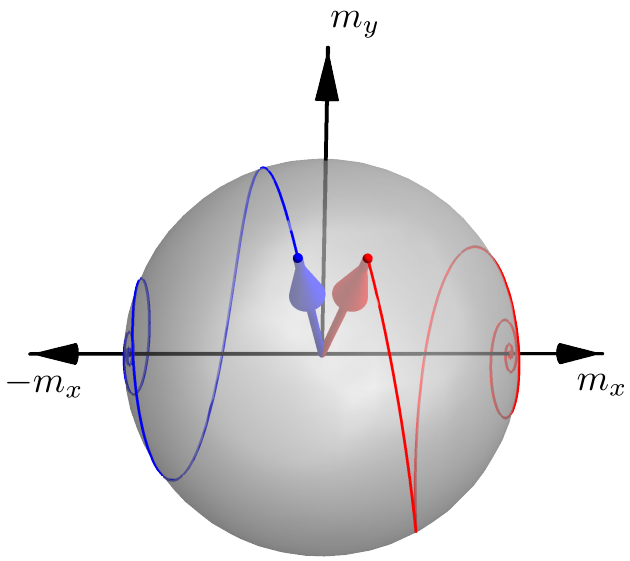

Figure 2.6: (Color online) Magnetization dynamics towards the points of lowest energy in the $\pm x$ directions. The parameters: $\alpha/A = 0.1$, $K_{uni}/A = 1.0[GHz]$, initial positions $\phi_i = \pi/16$ (red), $31\pi/16$ (blue), $\theta_i = \pi/4$.

The contact with topological edge states changes the energy profile of the 1D ferromagnet. The energy of the occupied electrons is controlled by the gap-openning terms: the larger the energy gap, the lower the electronic energy. The minimum energy corresponds to the magnetization that lies in the $x-z$ plane when the energy gap is maximized. We phenomenologically model this anisotropic energy in terms of $\varepsilon_{ti} = -K_{ti}\hat{m}_y^2 = -K_{ti}\cos^2\theta$ with $K_{it} < 0$, Fig. 2.7. The energy contours imply two types of magnetization motion in the absence of damping, dividing by the contour of zero energy. In the two

areas with the points of lowest energy enclosed, the magnetization still rotates around the x axis. In the upper and lower parts on the energy contour, the magnetization goes around the y axis.

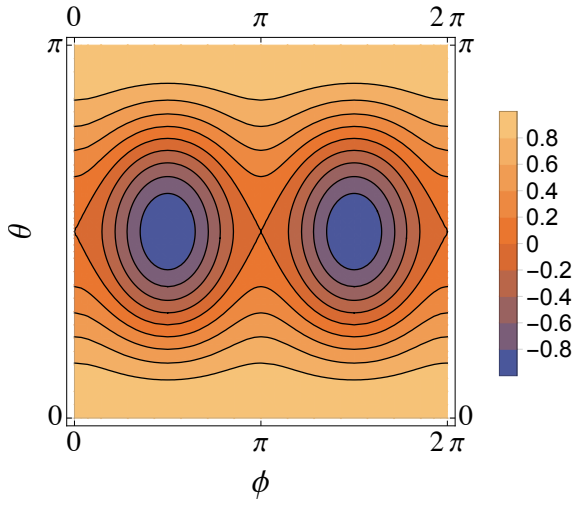

Figure 2.7: (Color online) The energy contour with the contribution from topological electrons ε_{ti}. The parameters: $K_{ti}/K_{uni} = -1$.

The magnetization equations of motion now reads,

$$\begin{pmatrix} 2\alpha & -A\sin\theta \\ A\sin\theta & 2\alpha\sin^2\theta \end{pmatrix} \begin{pmatrix} \dot{\theta} \\ \dot{\phi} \end{pmatrix} = \begin{pmatrix} -\partial(\varepsilon_{uni}+\varepsilon_{ti})/\partial\theta \\ -\partial(\varepsilon_{uni}+\varepsilon_{ti})/\partial\phi \end{pmatrix}. \tag{2.44}$$

where the Berry curvature term is renormalized as $A \to (1+\alpha/\pi)A$. The two lowest-energy positions are still in the x direction. However, the y-z plane is not the continental divider for initial states evolving to the two equilibrium positions. Magnetization on the energy contours around the x axis relaxes to the closest point of lowest energy. The final state of the magnetization on

energy contours around the y axis depends on the damping coefficients α. In Fig. 2.7, two points with $\theta_i = 0.3\pi, 0.7\pi$ evolve to different equilibrium points.

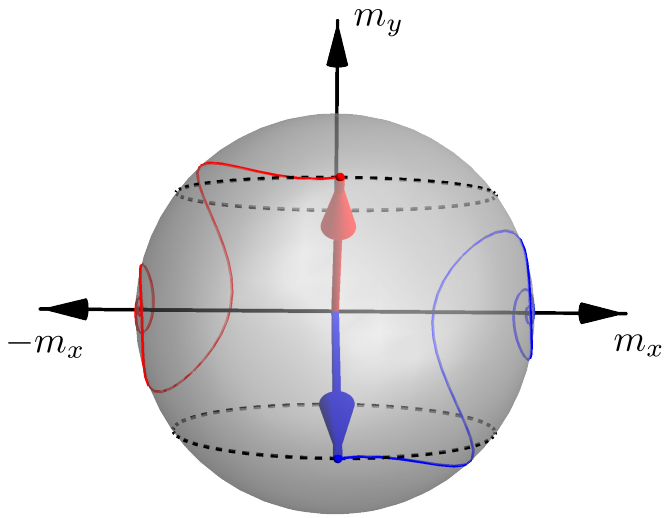

Figure 2.8: (Color online) Magnetization dynamics towards the lowest energy points in the $\pm x$ direction for ferromagnets in contact with TI. The parameters: $K_{ti}/K_{uni} = -1$, initial position $\phi_i = 0$, $\theta_i = 0.3\pi$ (red), 0.7π (blue).

In the presence of an electric field, the induced $\boldsymbol{H}^E$ tends to drive the magnetization rotating around the y axis. The energy dissipation due to Gilbert damping can be cancelled by the work density of the electric field, and thus changes the evolution on the magnetization sphere. Plugging $H_\phi^E = -eE/2\pi \sin\theta$ into the dynamical equations gives the equations of motion,

$$\begin{pmatrix} 2\alpha & -A\sin\theta \\ A\sin\theta & 2\alpha\sin^2\theta \end{pmatrix} \begin{pmatrix} \dot{\theta} \\ \dot{\phi} \end{pmatrix} = \begin{pmatrix} -\partial(\varepsilon_{uni}+\varepsilon_{ti})/\partial\theta \\ -\partial(\varepsilon_{uni}+\varepsilon_{ti})/\partial\phi \end{pmatrix} + \begin{pmatrix} 0 \\ -B\sin\theta \end{pmatrix}, \quad (2.45)$$

where $B = eE/2\pi$. From the simulation, the final position for the red trajectory is changed for $B/K_{uni} = 0.1$. The magnetization goes around the y axis for 3/4 circle before it relaxes to the point of lowest energy. With the positive electric work, the magnetization evolves to the other equilibrium point, see Fig. 2.9.

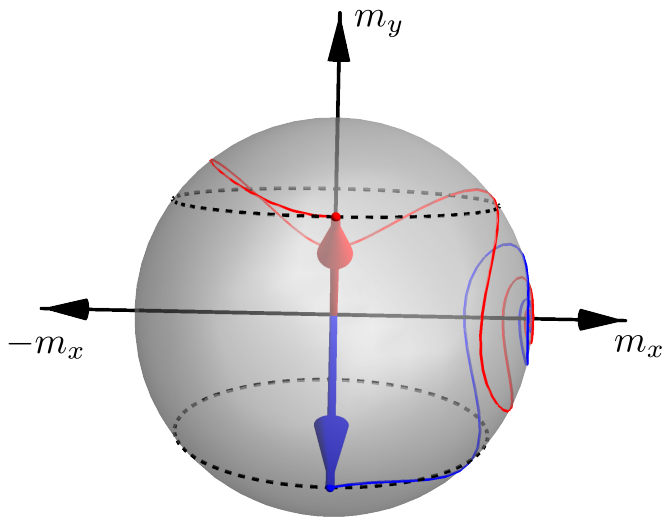

Figure 2.9: (Color online) Under an electric field, the Faraday $\boldsymbol{H}$ field drives the magnetization towards the other point of lowest energy. The parameters: $K_{ti}/K_{uni} = -1$,$B/K_{uni} = 0.1$, initial positions $\phi_i = 0$, $\theta_i = 0.3\pi$ (red), 0.7π (blue).

2.4.2 Spin-Torque Oscillators

The electric work cancels the energy dissipation, suggesting that a self-sustained oscillation on the magnetization sphere is possible, i.e. the oscillator state [58]. The electric work over a closed loop is nonzero if and only if the magnetization goes around the y axis. Therefore, a static magnetic field in the y direction is applied. As a result, the equilibrium position is shift in Fig. 2.10 and Fig. 2.11.

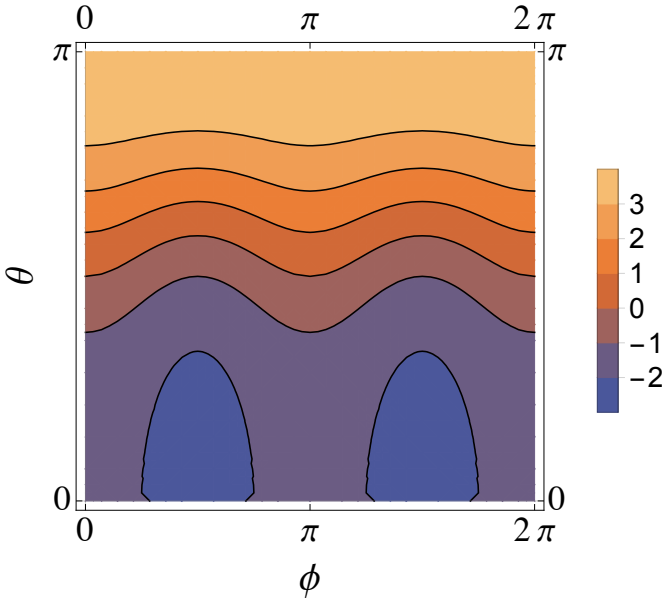

Figure 2.10: (Color online) The energy contour with a static magnetic field, $\varepsilon_H = -H\hat{m}_y^2$. The parameters: $K_{ti}/K_{uni} = -1$, $H/K_{uni} = 1$

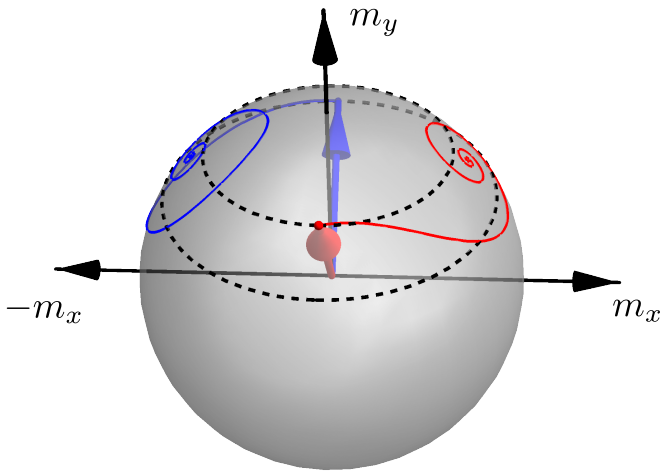

Figure 2.11: (Color online) The evolution on the magnetization sphere with a static magnetic field. The parameters: $H/K_{uni} = 1$, initial positions $\phi_i = 0$ (red), $\phi_i = \pi$ (blue), $\theta_i = 0.3\pi$.

In the following we only consider the case that the oscillator is on the positive y axis, and the angular velocity of magnetization rotation is positive along y axis. To obtain positive work density, the induced field should be along the direction of magnetization motion, $\boldsymbol{H}_{\phi}^{E} > 0$; hence, $B < 0$, and $E < 0$. With proper magnitudes of magnetic field, the stable oscillator state can be reached, Fig. 2.12. During one circle of motion, the electric work gives an energy input that cancels with the energy dissipation.

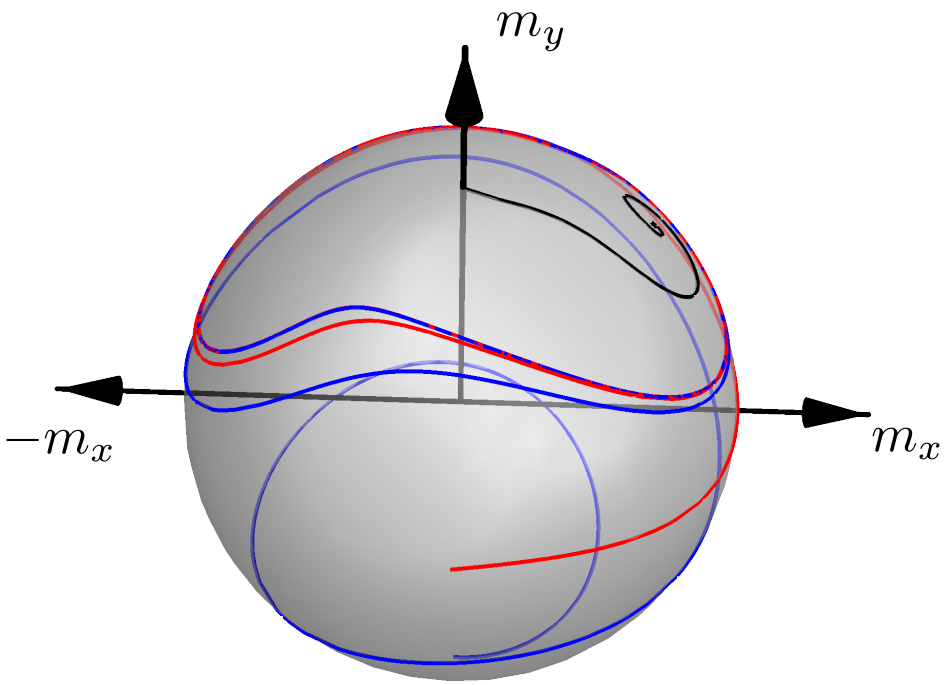

Figure 2.12: (Color online) The evolution on the magnetization sphere with an electric field and a static magnetic field. The parameters: $B/K_{uni} = -0.1$,$H/K_{uni} = 1$, initial positions $\theta_i = 0.001\pi$ (black), $\theta_i = 0.4\pi$ (red), $\theta_i = 0.8\pi$ (blue), $\phi_i = 0$.

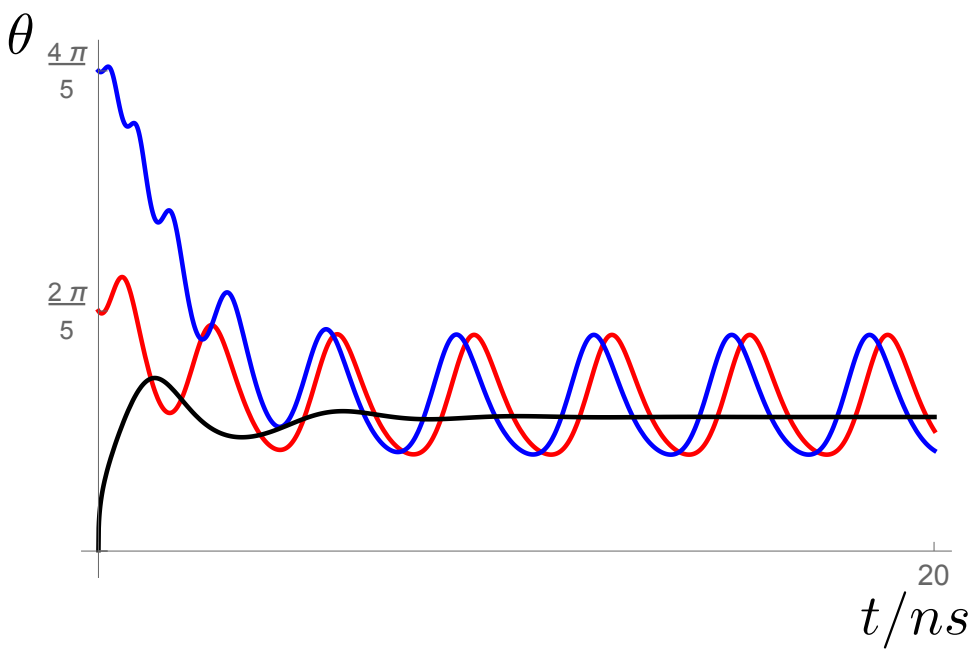

Figure 2.13: (Color online) The θ angle evolution. The red and blue lines are oscillator states. The purple line evolves to the point of lowest energy. The parameters: $B/K_{uni} = -0.1$,$H/K_{uni} = 1$, initial positions $\theta_i = 0.001\pi$ (black), $\theta_i = 0.4\pi$ (red), $\theta_i = 0.8\pi$ (blue), $\phi_i = 0$.

In Fig. 2.12, two different initial states of magnetization, the red and blue curve, go to the sustained state. The independence on the initial conditional implies that the oscillator state is stable against perturbations. The stability can be understood in terms of the net energy increase over one period, $\delta\varepsilon = W_{pumping} - W_{diss}$, which is the difference between the energy input via pumping $W_{pumping}$ and the energy dissipation W_{diss}. Note the pumping energy is quantized and thus fixed over one period. On the other hand, the energy dissipation is proportional to $\sin^2\theta$ and varies when trajectory extends

or shrinks (assuming fixed angular frequency). When the trajectory extends as θ increases, energy dissipation increases. The trajectory then goes back to the one with smaller θ (Fig. 2.10), which forms a negative-feedback system.

Chapter 3

Field-Induced Effects in Inhomogeneous Materials

In this chapter, the magnetization dynamics in inhomogeneous magnetic materials is discussed based on the second-order semiclassical theory of electrons, emphasizing the field-induced effects. First, we review the Dzyaloshinskii-Moriya Interactions (DMI) that stabilizes the chiral structures in non-uniform magnetic materials, such as chiral domain walls, Skyrmions and spiral structures. Next, we examine the charge-pumping current by magnetization motion in inhomogeneous materials, and obtain the geometric contribution in the field-induced torques using the reciprocal relation between the charge pumping and the field-induced torques. Then we introduce the semiclassical framework based on the wavepacket description of electrons in inhomogeneous systems. The electronic contribution to magnetization dynamics is obtained in terms of the effective $\boldsymbol{H}$ fields, from which we are able to identify the DMI in equilibrium and the DMI induced by electric fields. Notably, the geometric contribution in terms of the second Chern form provides a driven force to the magnetization dynamics. Finally, we illustrate the induced effective $\boldsymbol{H}$ fields with numerical calculations in TMD/FM systems.

3.1 Dzyaloshinskii-Moriya Interactions

Magnetic materials have domains of uniform magnetization and domain walls separating the domains. This is the result of different energies in the solids, for example, the exchange interaction, the anisotropic energy and the static magnetic energy. To understand the inhomogeneity of the magnetization, we first refer to Landau's phenomenological theory. The free energy of the system is assumed to be a functional of the magnetization (in the continuum limit). Stable configurations minimize the free energy, globally or locally, corresponds to the ground states and the metastable states of the system. For our purpose, the existence of the magnetization order is taken for granted (away from the phase transition point). Hence the uniform magnetization $\boldsymbol{m}_0$ is considered as the reference point for an inhomogeneous magnetization $\boldsymbol{m}(\boldsymbol{x})$. Assuming small inhomogeneity, the free energy is expanded in terms of magnetization gradients,

$$F[\boldsymbol{m}(\boldsymbol{x})] = F[\boldsymbol{m}_0] - T_{ij}\partial_i m_j + K_{ijkl}\partial_i m_j \partial_k m_l + \ldots, \tag{3.1}$$

with coefficients T_{ij} and K_{ij} for the linear and quadratic terms, respectively. The linear term vanishes if the system has inversion symmetry; otherwise the free energy changes sign as the magnetization reverses, $\partial_{\boldsymbol{x}}\boldsymbol{m} \to -\partial_{\boldsymbol{x}}\boldsymbol{m}$. The quadratic term is even under inversion operation and does not require inversion symmetry breaking. The magnitude of magnetization is assumed fixed because the longitudinal variation takes more energy than the transverse one does. With the assumption of stiff magnetization $\delta\boldsymbol{m} \perp \boldsymbol{m}$, the first term

is written in the form of Dzyaloshinskii-Moriya Interactions [59],

$$F_{DMI} = \boldsymbol{D}_i \cdot \partial_i \boldsymbol{m} \times \boldsymbol{m} = D_{ij}\epsilon_{jkl}\partial_i m_k m_l, \tag{3.2}$$

where the vector $\vec{D}_i$ is the DM vector in the direction i, and is related to the linear coefficients in Eq. (3.1) as $T_{ij} = (\boldsymbol{D}_i \times \boldsymbol{m})_j$.

To minimize energy, the magnetization direction tends to gradually rotate around the vector $\boldsymbol{D}_i$ as the space coordinates move along the direction i. The energetic preferred magnetization configuration can thus be obtained if the DM vectors, as function of magnetization, are known. Some special forms of DM vectors generate interesting magnetic structures observed in experiments. For example, the Bloch type domain wall is preferred in structure with a symmetric D_{ij} matrix, where the DM vectors aer along the direction of the coordinates variation. On the other hand, an antisymmetric D_{ij} matrix prefers the Neel type structure, where the DM vectors are perpendicular to the direction of the coordinates variation. In Fig. 3.1(a,b), two Neel type DW's are shown with opposite DM vectors. In Fig. 3.2, two types of Skyrmions are presented with antisymmetric and symmetric D_{ij}'s, respectively.

To understand the phenomenological free energy, we assume the magnetization is all from the spin and consider the spin lattice models. The linear term and quadratic term have microscopic correspondence in the spin-spin interaction, namely, the antisymmetric and symmetric exchange coupling, respectively, in the following spin Hamiltonian,

$$\hat{H} = \sum_{ij}(-J_s\vec{S}_i \cdot \vec{S}_j - \vec{J}_a \cdot \vec{S}_i \times \vec{S}_j), \tag{3.3}$$

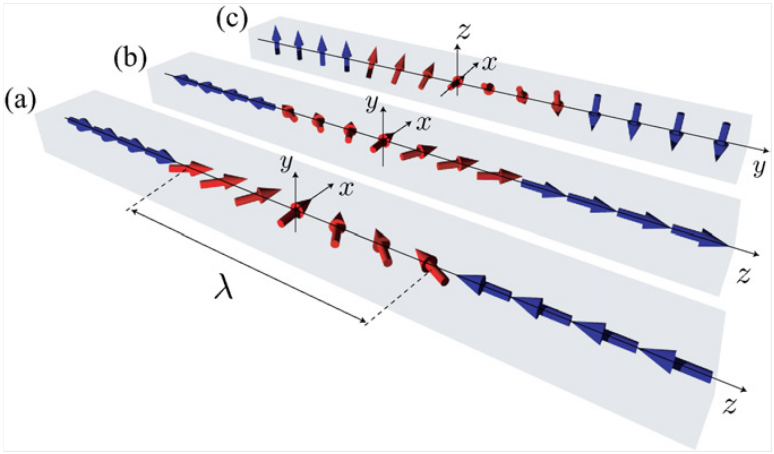

Figure 3.1: (Color online) The domain wall of (a) Neel type with DM vector $\vec{D}_z = \hat{e}_y$, (b) Neel type with $\vec{D}_z = -\hat{e}_y$, (c) Bloch type with $\vec{D}_y = -\hat{e}_y$. Adapted from Ref. [3]

Figure 3.2: (Color online) Skyrmion of (a) Neel type $\vec{D}_r = -\hat{e}_\phi$, (b) Bloch type $\vec{D}_r = -\hat{e}_r$. Adapted from Ref. [4]

where S_i labels the spin on site i, J_s and J_a are the exchange coupling constants. The antisymmetric interaction derives from the superexchange interactions in materials with spin-orbital coupling [60]. The exchange interaction depends on the hopping direction of electrons due to SOC. Thus the coupling coefficients should change sign as the two neighboring spins switch site, giving

the antisymmetric form in Eq. (3.3).

On the mean field level, the effective fields on the spin from the antisymmetric exchange coupling is proportional to the spatial gradients of spin,

$$\vec{h} = \vec{J}_a^i \times \nabla_i \vec{S}, \tag{3.4}$$

where i labels the spatial direction. Compared with Eq. (3.1), this is exactly the linear term in the phenomenological free energy. The DMI coefficient can be extracted from the effective fields by terms that (1) are linear in the gradient of magnetization, and (2) are antisymmetric in the magnetization indexes. In the following sections, we use the semiclassical framework to derive the equation of motion for the inhomogeneous magnetization, from which the DMI can be extracted from the effective fields using these two features.

3.2 Adiabatic Charge Pumping in Inhomogeneous Materials

The Onsager reciprocal relation between the charge-pumping current by magnetization motion and the spin torques by electric fields has been confirmed for uniform magnetic materials. We are motivated to study the charge-pumping current in the presence of inhomogeneity, for the purpose of investigating the electric field-induced torques in non-uniform magnetic materials.

The reciprocal relation can be understood from the aspect of energy transfer between electric fields and electrons. On the one hand, the electric field does mechanical work to the electron system, with the power density $P =$

$\boldsymbol{j}_p \cdot \boldsymbol{E}$, where $\boldsymbol{j}_p$ is the charge-pumping current by magnetization motion. On the other hand, the electronic energy changes as a function of magnetization, with the energy variation rate $dG/dt = \boldsymbol{H}^E \cdot \dot{\boldsymbol{m}}$, where $\boldsymbol{H}^E$ is the induced effective field on magnetization. In deriving the above relation, one times $\dot{\boldsymbol{m}}$ on the dynamical equation and ignores the energy dissipation. For non-dissipative systems, the energy conservation law implies that the electric work is equal to the energy gain of electrons,

$$\boldsymbol{j}_p \cdot \boldsymbol{E} = \boldsymbol{H}^E \cdot \dot{\boldsymbol{m}}. \tag{3.5}$$

The adiabatic charge pumping is non-dissipative; thus we can apply the energy conservation law to discuss the induced effective fields in inhomogeneous systems. For solids driven by a slowly varying parameter λ, the adiabatic current is written as,

$$\boldsymbol{j} = e \int [d\boldsymbol{k}] \Omega_{\boldsymbol{k}\lambda} \dot{\lambda} dt, \tag{3.6}$$

where $\boldsymbol{k}$ is the crystal momentum, $\Omega_{\boldsymbol{k}\lambda} = \partial_{\boldsymbol{k}} A_\lambda - \partial_\lambda A_{\boldsymbol{k}}$ is the Berry curvature. This adiabatic current corresponds to the intrinsic contribution to the spin-orbital torque discussed in Chapter 2.

In the wavepacket representation, the current is obtained by summing over all the wavepacket contribution,

$$\boldsymbol{j}(\boldsymbol{r}) = \int [d\boldsymbol{k}_c d\boldsymbol{r}_c] \cdot g(\boldsymbol{k}_c, \boldsymbol{r}_c) \langle W | \dot{\hat{\boldsymbol{r}}} \delta(\hat{\boldsymbol{r}} - \boldsymbol{r}) | W \rangle. \tag{3.7}$$

where $\boldsymbol{k}_c$ and $\boldsymbol{r}_c$ represent wavepacket center momentum and position and g is the distribution function. Since the wavepacket is well localized around

the center position $\boldsymbol{r}_c$, it is plausible to expand the delta function around the wavepacket center $\boldsymbol{r}_c$ [61], $\delta(\hat{\boldsymbol{r}}-\boldsymbol{r}) = \delta(\boldsymbol{r}_c-\boldsymbol{r}) - (\hat{\boldsymbol{r}}-\boldsymbol{r}_c)\nabla_{\boldsymbol{r}}\delta(\boldsymbol{r}_c-\boldsymbol{r})$. Plugging it into the current expression gives,

$$\boldsymbol{j}(\boldsymbol{r}) = \int [d\boldsymbol{k}] \cdot g(\boldsymbol{k},\boldsymbol{r})\dot{\boldsymbol{r}} + \nabla_{\boldsymbol{r}} \times \int [d\boldsymbol{k}] \cdot g\boldsymbol{m}, \tag{3.8}$$

which contains the center of mass motion, and the curl of the local magnetization associated with the wavepacket.

The total current $\boldsymbol{j}$ is not the transport current measured in the conventional transport experiments [62]. Specifically, when the scale of measurements is larger than the scale of local equilibrium states, the magnetization contribution should be subtracted [63]. From an experimental point of view, the device of large scale resolution is neutral to the dipoles, for example, the magnetization. Nonetheless, dipole is a real physical quantity instead of gauge effects. It can be measured when the resolution of measurements is comparable to the scale of equilibrium states.

Substituting the velocity of wavepacket center, and subtracting the magnetization contribution, the transport current is obtained,

$$\begin{aligned} \boldsymbol{j}_{tr} &= \boldsymbol{j} - \nabla_{\boldsymbol{r}} \times \boldsymbol{M} && (3.9)\\ &= (-e) \cdot \int [d\boldsymbol{k}] f_0 [\frac{\partial \varepsilon}{\partial \boldsymbol{k}} - \Omega_{\boldsymbol{k}t}] && (3.10)\\ &\quad + f_0 [\Omega_{\boldsymbol{k}\boldsymbol{x}} \cdot \Omega_{\boldsymbol{k}t} - \Omega_{\boldsymbol{k}\boldsymbol{k}} \cdot \Omega_{\boldsymbol{x}t} - \Omega_{\boldsymbol{k}t} Tr \Omega_{\boldsymbol{k}\boldsymbol{x}}], && (3.11) \end{aligned}$$

where the dot product is on neighboring index $\boldsymbol{k}$ and $\boldsymbol{x}$. The first line contains the energy gradient and the charge-pumping current for uniform materials.

The second line is the charge-pumping current in the presence of inhomogeneity. It has been used to derive the charge distribution in inhomogeneous magnetization textures [64]. The electromagnetic coupling in topological insulators is derived by taking the inhomogeneity from electromagnetic fields $\boldsymbol{A}(\boldsymbol{x})$.

With the charge-pumping current, we write down the induced effective fields using the reciprocal relation,

$$\boldsymbol{H}^E = -e\boldsymbol{E} \cdot \int f_0[d\boldsymbol{k}][\Omega_{\boldsymbol{kx}} \cdot \Omega_{\boldsymbol{km}} - \Omega_{\boldsymbol{kk}} \cdot \Omega_{\boldsymbol{xm}} - \Omega_{\boldsymbol{km}} Tr \Omega_{\boldsymbol{km}}]. \tag{3.12}$$

The spatial gradient is through the magnetization, $\partial/\partial\boldsymbol{x} = \partial\boldsymbol{m}/\partial\boldsymbol{x} \cdot \partial/\partial\boldsymbol{m}$. Due to the total antisymmetric indexes of the second Chern form, we have the following inferences. First, the minimal dimension of the electronic Hamiltonian that supports nonzero second Chern form is two. Second, the electric field couples with the gradient only in the perpendicular direction.

In the absence of SOC, only the second term in Eq. (3.12) survives. For ferromagnets with the *sd* model, the Berry curvature is $\Omega_{\boldsymbol{m}} = \boldsymbol{m}/2m^3$ in the vector form. Plugging it into the effective fields, we obtain

$$\boldsymbol{H}^E = \boldsymbol{j} \cdot \Omega_{\boldsymbol{xm}} = \frac{1}{2m^3} \boldsymbol{m} \times (\boldsymbol{j} \cdot \nabla \boldsymbol{m}), \tag{3.13}$$

where $\boldsymbol{j}_i = \sigma_{ij} E_j$ is the Hall current and $\sigma_{ij} = \frac{e^2}{\hbar} \int f_0[dk] \Omega_{k_i k_j}$ is the Hall conductivity. Eq. (3.13) suggests that the effective fields originate from the mismatch between the local magnetization and the electronic spin. The electrons mediate torques to align the magnetization, as it is traveling in inhomo-

geneous material, which agrees with the momentum transfer picture [6]. The current-mediated mechanism applies for the non-adiabatic current as well.

3.3 Semiclassical Framework for Non-uniform Magnetization Dynamics

Electric fields have been used to tune the spatial profile of magnetization textures and control the motion of domain walls and Skyrmions[65]. The effects of electric fields and magnetization gradients have been proposed in metals with weak spin-orbital coupling [6], where the non-equilibrium electron mediates the transfer of angular momentum between magnetizations (RKKY).

To obtain a semiclassical theory of magnetization dynamics with inhomogeneity and electric fields, the second-order wavepacket methods should be used. In the following, we introduce the second-order methods and present the electronic contribution in the effective fields in terms of the field-induced DMI and the geometric second Chern form.

3.3.1 The Perturbed Wavepacket

We start from the construction of the wavepackets in the semiclassical framework. The wavepacket is well localized in space compared with length scale of magnetization $\boldsymbol{m}(\boldsymbol{x})$. Hence the electronic Hamiltonian is expanded around the wavepacket center $\boldsymbol{x}_c$,

$$\hat{H} = \hat{H}_c + \hat{H}' + \hat{H}'', \tag{3.14}$$

where H' and H'' are the first-order and second-order perturbations in $(\hat{\boldsymbol{x}}-\boldsymbol{x}_c)$. The local Hamiltonian is obtained by evaluating the magnetization at the center position of the wavepacket,

$$\hat{H}_c = H_0 - J\hat{\boldsymbol{\sigma}} \cdot \boldsymbol{m}(\boldsymbol{x}_c, t) + \boldsymbol{E} \cdot \boldsymbol{x}_c. \tag{3.15}$$

where $\hat{\boldsymbol{\sigma}}$ is the electron spin operator, and J is the exchange coupling constant. For convenience, we set $J = 1$ in the following derivation. The electric field contributes a constant thus does not affect the Bloch states. Note $\hat{H}_c$ recovers the translation symmetry; hence the crystal momentum $\boldsymbol{p}$ is well defined locally. In the first-order semiclassical theory, the wavepacket is constructed using the Bloch states $|\psi_{0\boldsymbol{p}}\rangle = e^{i\boldsymbol{p}\cdot\boldsymbol{x}}|u_0\rangle$ with

$$|W\rangle = \int [d\boldsymbol{p}] \cdot C_0(\boldsymbol{p})|\psi_{0\boldsymbol{p}}\rangle, \tag{3.16}$$

where C_0 is the superposition coefficient centered in momentum $\boldsymbol{p}_c$, and the subscript 0 labels the band.

In the second-order semiclassical theory, the wavepacket is constructed with the perturbed Bloch states,

$$|\widetilde{\psi}_{0\boldsymbol{p}}\rangle = |\psi_{0\boldsymbol{p}}\rangle + \int [d\boldsymbol{p}_1] \cdot \sum_n \frac{\langle\psi_{n\boldsymbol{p}_1}|H'|\psi_{0\boldsymbol{p}}\rangle}{\varepsilon_{0\boldsymbol{p}} - \varepsilon_{n\boldsymbol{p}_1}}|\psi_{n\boldsymbol{p}_1}\rangle, \tag{3.17}$$

where the perturbed Hamiltonian H' for magnetization gradients is,

$$H'_m = -\frac{\partial \boldsymbol{m}}{\partial \boldsymbol{x}}|_c \cdot \hat{\boldsymbol{\sigma}}(\hat{\boldsymbol{x}} - \boldsymbol{x}_c), \tag{3.18}$$

and for the electric field,

$$H'_E = \boldsymbol{E} \cdot (\hat{\boldsymbol{x}} - \boldsymbol{x}_c). \tag{3.19}$$

Because the position operator $\hat{\boldsymbol{x}}$ breaks the translational symmetry, the perturbed states are mixtures of Bloch states with multiple crystal momentums. In the weak field limit, the perturbed Bloch states have one-to-one correspondence from the unperturbed ones,

$$|\psi_{0\boldsymbol{p}}\rangle \to |\widetilde{\psi}_{0\boldsymbol{p}}\rangle. \tag{3.20}$$

The perturbed Bloch states form the perturbed manifold in the Brillouin zone. Essentially, the second-order theory is obtained by replacing the unperturbed manifold with the perturbed one in the first-order theory. As results, they share similar structures in the Lagrangian and equations of motion of the wavepackets.

To express the perturbation effects explicitly, it is useful to work in the unperturbed Bloch states. By combining terms with the phase factor $e^{i\boldsymbol{p}\cdot\boldsymbol{x}}$, the wavepacket is presented in the unperturbed states,

$$|W\rangle = \int [d\boldsymbol{p}] \cdot e^{i\boldsymbol{p}\cdot\boldsymbol{x}} \big[C_0(\boldsymbol{p})|u_{0\boldsymbol{p}}\rangle + \sum_{n\neq 0} C_n(\boldsymbol{p})|u_{n\boldsymbol{p}}\rangle\big], \tag{3.21}$$

with the coefficients,

$$C_n = \int [d\boldsymbol{p}_1] C_0(\boldsymbol{p}_1) \frac{\langle \psi_{n\boldsymbol{p}}|H'_s|\psi_{0\boldsymbol{p}_1}\rangle}{\varepsilon_{0\boldsymbol{p}_1} - \varepsilon_{n\boldsymbol{p}}}. \tag{3.22}$$

The second part of the wavepacket is linear in external perturbations, giving rise to all the second-order effects.

Substituting the H' in Eq. (3.22), we obtain the coefficients in the presence of electric fields,

$$C_{\boldsymbol{E},n}(\boldsymbol{p}) = \frac{\boldsymbol{E}\cdot\boldsymbol{A}_{n0}}{\varepsilon_0 - \varepsilon_n} C_0(\boldsymbol{p}) \tag{3.23}$$

where the interband Berry connection $\boldsymbol{A}_{n0} = \langle u_n | i\partial_{\boldsymbol{p}} | u_0 \rangle$. We have simplified the notation by omitting the $\boldsymbol{p}$ argument, $\varepsilon_{0\boldsymbol{p}} \to \varepsilon_0$. For magnetization gradients, we obtain

$$\begin{aligned} C_{\boldsymbol{m},n}(\boldsymbol{p}) &= -\frac{\partial \boldsymbol{m}}{\partial \boldsymbol{x}} \cdot \big[-\partial_{\boldsymbol{p}} C_0(\boldsymbol{q}) \boldsymbol{A}^m_{n0} \\ &\quad + \frac{\boldsymbol{v}_0}{\varepsilon_0 - \varepsilon_n} C_0 \boldsymbol{A}^m_{n0} + \sum_{n_2} C_0 \frac{\boldsymbol{\sigma}_{nn_2} \boldsymbol{A}_{n_2 0}}{\varepsilon_0 - \varepsilon_n} - i C_0 \boldsymbol{x}_c \boldsymbol{A}^m_{n0} \big] \\ &= -\frac{\partial \boldsymbol{m}}{\partial \boldsymbol{x}} \cdot i(i\boldsymbol{\partial}_{\boldsymbol{p}} + \boldsymbol{a}_0 - \boldsymbol{x}_c) C_0 \boldsymbol{A}^m_{n0} + \frac{\boldsymbol{G}_{n0}}{\varepsilon_0 - \varepsilon_n} C_0. \end{aligned} \tag{3.24}$$

where $\boldsymbol{G}_{n0} = -\frac{\partial \boldsymbol{m}}{\partial \boldsymbol{x}} \cdot \boldsymbol{Q}_{n0}$, and $\boldsymbol{Q}_{n0} = \boldsymbol{v}_0 \boldsymbol{A}^m_{n0} + \sum_{n_2 \neq 0} \boldsymbol{\sigma}_{nn_2} \boldsymbol{A}_{n_2 0}$. We have used the interband Berry connection in momentum $\boldsymbol{A}_{n0} = \langle u_n | i\partial_{\boldsymbol{p}} | u_0 \rangle$, the interband Berry connection in magnetization $\boldsymbol{A}^m_{n0} = \langle u_n | i\partial_{\boldsymbol{m}} | u_0 \rangle$, and $\boldsymbol{a}_0 = \boldsymbol{A}_{00}$, $\boldsymbol{v}_0 = \partial_{\boldsymbol{p}} \varepsilon_0$. The Berry connections without superscript are with respect to the crystal momentum.

Expressed in the unperturbed Bloch states, the wavepacket contains Bloch states of other bands (in the *vertical* directions) and of other positions (in the *horizontal* directions). In contrast, the first-order theory constructs the wavepacket with the Bloch states only in the same band at the same position. Specifically, the second term in C_n represents the mixing of the Bloch states from different bands. $\boldsymbol{G}_{n0}$ contains the interband matrix elements of the spin dipole moments $\boldsymbol{Q}_{n0}$ that couples with the magnetization gradient $-\frac{\partial \boldsymbol{m}}{\partial \boldsymbol{x}}$. The first term in $\boldsymbol{G}_{n0}$ is an adiabatic contribution from the Berry phase effect. The second term in $\boldsymbol{G}_{n0}$ is a non-adiabatic effect and involves scattering in intermediate states.

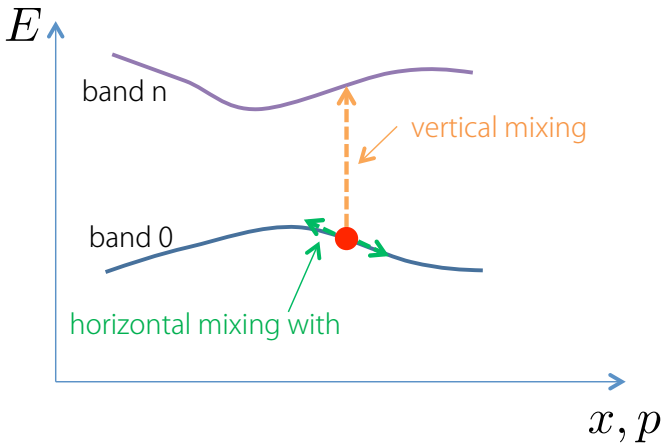

Figure 3.3: (Color online) Schematic plot of the vertical and horizontal mixing of the wavepacket. Adapted with modification from Ref. [5]

The first term in C_n represents the mixing from the Bloch states around the center position and center momentum. To clarify this point, the particular perturbation in wavepacket is written as,

$$\begin{aligned} & -\frac{\partial \boldsymbol{m}}{\partial \boldsymbol{x}}|_c \cdot \int [d\boldsymbol{p}] e^{i\boldsymbol{p}\cdot\boldsymbol{x}} i(i\boldsymbol{\partial} + \boldsymbol{a}_0 - \boldsymbol{x}_c) C_0 \sum_{n\neq 0} \boldsymbol{A}^m_{n0} |u_n\rangle \\ = & \int [d\boldsymbol{p}] e^{i\boldsymbol{p}\cdot\boldsymbol{x}} \frac{\partial \boldsymbol{m}}{\partial \boldsymbol{x}}|_c \cdot (\hat{\boldsymbol{x}} - \boldsymbol{x}_c) C_0 \hat{\boldsymbol{D}}_{\boldsymbol{m}} |u_0\rangle - C_0 i \frac{\partial \boldsymbol{m}}{\partial \boldsymbol{x}}|_c \hat{\boldsymbol{D}}_{\boldsymbol{p}} \hat{\boldsymbol{D}}_{\boldsymbol{m}} |u_0\rangle \\ = & \int [d\boldsymbol{p}] e^{i\boldsymbol{p}\cdot\boldsymbol{x}} C_0 |u_0(\boldsymbol{M}(\hat{\boldsymbol{x}})\rangle - C_0 i \frac{\partial \boldsymbol{m}}{\partial \boldsymbol{x}}|_c \hat{\boldsymbol{D}}_{\boldsymbol{p}} \hat{\boldsymbol{D}}_{\boldsymbol{m}} |u_0\rangle, \end{aligned} \tag{3.25}$$

where the gauge-invariant differential operator $\hat{\boldsymbol{D}}_{\boldsymbol{m}} = (\partial_{\boldsymbol{m}} + i\boldsymbol{a}_m)$ and $\hat{\boldsymbol{D}}_{\boldsymbol{p}} = (\partial_{\boldsymbol{p}} + i\boldsymbol{a}_0)$ with $\boldsymbol{a}_m = \boldsymbol{A}^m_{00}$. The smearing round center position is the first term, $(\hat{\boldsymbol{x}} - \boldsymbol{x}_c)\boldsymbol{D}_{\boldsymbol{x}}$, $(\boldsymbol{D}_{\boldsymbol{x}} = \partial_{\boldsymbol{x}}\boldsymbol{m} \cdot \boldsymbol{D}_{\boldsymbol{m}})$. The second term presents the mixtures in both momentum and real space on the zero band manifold.

3.3.2 Positional Shift of Wavepacket

The center position of the wavepacket is perturbed by electric fields and magnetization gradients. The center position of the perturbed wavepacket is,

$$\boldsymbol{r}_c = \langle W|\hat{\boldsymbol{x}}|W\rangle = \int [d\boldsymbol{p}] C_0^* i\partial_{\boldsymbol{p}} C_0 + \tilde{\boldsymbol{a}}_0, \tag{3.26}$$

where the corrected Berry connection $\tilde{\boldsymbol{a}}_0 = \int [d\boldsymbol{p}]|C_0|^2 \boldsymbol{a}_{0,\boldsymbol{p}} + C_n^* C_0 \boldsymbol{A}_{n0,\boldsymbol{p}} + C_0^* C_n \boldsymbol{A}_{0n,\boldsymbol{p}}$. After some tedious derivation, the corrected Berry connection is refined as,

$$\tilde{\boldsymbol{a}}_{0,i} = \boldsymbol{a}_{0,i} + \alpha_{ij}\boldsymbol{E}_j + \beta_{ijk}\frac{\partial \boldsymbol{m}_k}{\partial \boldsymbol{x}_j}. \tag{3.27}$$

with coefficients,

$$\alpha_{ij} = e \cdot \sum_{n\neq 0} \frac{V_{0n}^i V_{n0}^j}{(\varepsilon_0 - \varepsilon_n)^3} + c.c, \tag{3.28}$$

and

$$\beta_{ijk} = \sum_{n\neq 0} \partial_{p_j}[\sigma_{n0}^k V_{0n}^i / 2(\varepsilon_0 - \varepsilon_n)^2] + \sum_{n\neq 0} i Q_{n0}^{jk} \cdot V_{0n}^i / (\varepsilon_0 - \varepsilon_n)^2 + c.c. \tag{3.29}$$

where $\boldsymbol{V}_{n0} = \langle u_n|\hat{\boldsymbol{V}}|u_0\rangle$, and $\hat{\boldsymbol{V}} = \partial \hat{H}_c/\partial \boldsymbol{p}$ is the velocity operator, $\boldsymbol{\sigma}_{n0} = \langle u_n|\hat{\boldsymbol{\sigma}}|u_0\rangle$, and $v_0^i = V_{00}^i$. The second and third term are the positional shift by $\boldsymbol{E}$ fields and magnetization gradients $\partial \boldsymbol{m}/\partial \boldsymbol{x}$, respectively.

3.3.3 Adiabatic Evolution of Wavepacket

When the perturbed manifold is mapped from the unperturbed one, the energy gap is still larger than the time variation rates of parameters in the electronic Hamiltonian. Hence the quantum mechanical evolution of wavefunction is still adiabatic on the perturbed manifold. As in the first-order theory,

the adiabatic evolution on the perturbed manifold is obtained by using the following Lagrangian and applying the variational principle in the confined space,

$$\mathcal{L} = \langle W | i\frac{d}{dt} - \hat{H} | W \rangle / \langle W | W \rangle. \tag{3.30}$$

where the normalization of wavepacket is used. The wavepacket evolution is effectively the evolution of the coefficient. The following calculation aims to write the Lagrangian in terms of C_0 and its derivatives. Keeping to the second order, the Lagrangian is written as

$$\mathcal{L} = \int [d\boldsymbol{p}] C_0^* i\partial_t C_0 + \frac{d\boldsymbol{m}}{dt} \cdot \tilde{\boldsymbol{a}}^m - \tilde{\varepsilon}, \tag{3.31}$$

where $\tilde{\boldsymbol{a}}^m = \int [dp] |C_0|^2 \boldsymbol{a}_0^m + C_n^* C_0 \boldsymbol{A}_{n0}^m + C_0^* C_n \boldsymbol{A}_{0n}^m$ is the corrected Berry connection with respect to $\boldsymbol{m}$. After some tedious calculations, it is refined as,

$$\tilde{\boldsymbol{a}}_i^m = \boldsymbol{a}_i^m + \gamma_{ij} \boldsymbol{E}_j + \eta_{ijk} \frac{\partial \boldsymbol{m}_k}{\partial \boldsymbol{x}_j}, \tag{3.32}$$

with coefficients,

$$\gamma_{ij} = -e \cdot \sum_{n \neq 0} \frac{\sigma_{0n}^i V_{n0}^j}{(\varepsilon_0 - \varepsilon_n)^3} + c.c, \tag{3.33}$$

and

$$\eta_{ijk} = -\sum_{n \neq 0} \partial_{p_j} [\sigma_{n0}^k \sigma_{0n}^i / 2(\varepsilon_0 - \varepsilon_n)^2] - \sum_{n \neq 0} i Q_{n0}^{jk} \cdot \sigma_{0n}^i / (\varepsilon_0 - \varepsilon_n)^2 + c.c. \tag{3.34}$$

One can observe that γ_{ij}, η_{ijk} can be obtained from α_{ij}, β_{ijk} by replacing $\hat{\boldsymbol{V}} \to -\hat{\boldsymbol{\sigma}}$ in the expression, which suggests that the correction $\delta\boldsymbol{\sigma} = \tilde{\boldsymbol{a}}^m - \boldsymbol{a}^m$ is the correction of wavepacket spin orientation.

3.3.4 Effective Energy of Wavepacket

The second-order wavepacket energy is $\tilde{\varepsilon} = \varepsilon(1+2\delta) + \mathcal{L}_{dyn}$, with the dynamical energy $\mathcal{L}_{dyn} = -\int[d\boldsymbol{p}][2\delta \cdot C_0^* i\partial_t C_0 + C_n^* i\partial_t C_n]$. We first explain the origin of the dynamical energy $\mathcal{L}_{dyn}$. The total time derivative in the Lagrangian in Eq. (3.30) is,

$$\langle W|i\frac{d}{dt}|W\rangle = C_0^* i\partial_t C_0 + C_n^* i\partial_t C_n + C_n^* C_0 A_{n0}^t + C_0^* C_n A_{0n}^t + |C_0|^2 a_0^t + |C_n|^2 a_n^t, \tag{3.35}$$

where superscript t in the Berry connection denotes the total time derivative through magnetization $\boldsymbol{m}(\boldsymbol{x},t)$, $d_t = [\dot{\boldsymbol{x}}\partial_{\boldsymbol{x}}\boldsymbol{m} + \dot{\boldsymbol{m}}] \cdot \partial_{\boldsymbol{m}} = d_t\boldsymbol{m} \cdot \partial_{\boldsymbol{m}}$. Let us check the order of these terms in Eq. (3.35). The last term is a third order effect $\sim O(3)$; thus it is omitted. The first term has $O(0)$ order; the third to fifth term have $O(2)$ order – They are kept in the final expression of the Lagrangian Eq. (3.31). However, the second term has $O(2)$ order, and is put in the dynamical energy, $\mathcal{L}_{dyn,1} = -\int[d\boldsymbol{p}]C_n^* i\partial_t C_n$. In fact, the second term is related to C_0 and its derivatives, $\partial_{\boldsymbol{p}}C_0$ and $\partial_t C_0$. In the calculation below, we take $i\partial_t C_0 \approx \varepsilon_0 C_0$ and $i\partial_t C_n \approx \varepsilon_0 C_n$ in the Lagrangian. This is an approximation and the obtained energy is the effective energy of wavepacket to the second order. The other contribution in the dynamical energy $\mathcal{L}_{dyn,2} = -\int[d\boldsymbol{p}]2\delta C_0^* i\partial_t C_0$ is from the normalization relation,

$$\begin{aligned} \langle W|W\rangle &= \int[d\boldsymbol{p}]|C_0|^2 + |C_{\boldsymbol{E},n} + C_{\boldsymbol{m},n}|^2 \\ &= \int[d\boldsymbol{p}]|C_0|^2 + (C_{\boldsymbol{E},n}^* C_{\boldsymbol{m},n} + c.c) \\ &= (1+\delta)^{-2}, \end{aligned} \tag{3.36}$$

where $-2\delta = \int [d\boldsymbol{p}] C^*_{\boldsymbol{E},n} C_{\boldsymbol{m},n} + c.c.$ is the normalization factor. Combining with the $O(0)$ term in Eq. (3.35) gives the $\mathcal{L}_{dyn,2}$ term.

Next, we evaluate the dynamical energy $\mathcal{L}_{dyn} = -\int [d\boldsymbol{p}][2\delta C_0^* i\partial_t C_0 + C_n^* i\partial_t C_n]$ with $C_n = C_{\boldsymbol{E},n} + C_{\boldsymbol{m},n}$. Using the construction coefficients, for the magnetization perturbation part we have,

$$\begin{aligned} i\partial_t C_{\boldsymbol{m},n} &= -\frac{\partial \boldsymbol{m}}{\partial \boldsymbol{x}}|_c \cdot i(i\boldsymbol{\partial}_{\boldsymbol{p}} + \boldsymbol{a}_0 - \boldsymbol{x}_c) C_0 \boldsymbol{A}^m_{n0} \cdot \varepsilon_0 + \frac{G_{n0}}{\varepsilon_0 - \varepsilon_n} C_0 \cdot \varepsilon_0 \\ &\quad -\frac{\partial \boldsymbol{m}}{\partial \boldsymbol{x}}|_c \cdot i(i\boldsymbol{v}_0 - i\dot{\boldsymbol{x}}_c) C_0 \boldsymbol{A}^m_{n0} \\ &= \varepsilon_0 C_{\boldsymbol{m},n} + \frac{\partial \boldsymbol{m}}{\partial \boldsymbol{x}}|_c \cdot (\boldsymbol{v}_0 - \dot{\boldsymbol{x}}_c) C_0 \boldsymbol{A}^m_{n0}. \end{aligned} \tag{3.37}$$

The second term is taking to be zero in the first order because $\dot{\boldsymbol{x}}_c = \boldsymbol{v}_0 + O(1)$. For the electric field perturbation part we have,

$$i\partial_t C_{\boldsymbol{E},n} = \varepsilon_0 C_{\boldsymbol{E},n}. \tag{3.38}$$

There is no horizontal mixing in $C_{\boldsymbol{E},n}$; thus no extra term exists as in $i\partial_t C_{\boldsymbol{m},n}$. With these results, we have the dynamical energy,

$$\mathcal{L}_{dyn} = -\int [d\boldsymbol{p}][2\delta \cdot |C_0|^2 \varepsilon_0 + (C^*_{\boldsymbol{E},n} C_{\boldsymbol{m},n} + c.c)\varepsilon_0] = -\delta\varepsilon. \tag{3.39}$$

Now we move to the calculation of the energy from the Hamiltonian. To the second order, it contains three contributions. The first part is from the local Hamiltonian,

$$\begin{aligned} \langle W|\hat{H}_c|W\rangle(1+2\delta) &= \int [d\boldsymbol{p}][|C_0|^2\varepsilon_0 + |C_n|^2\varepsilon_n + 2\delta \cdot |C_0|^2\varepsilon_0] \\ &= \varepsilon_0 + \int [d\boldsymbol{p}]|C_n|^2(\varepsilon_n - \varepsilon_0) + \delta\varepsilon \\ &= \varepsilon_0 - \boldsymbol{E}_i \frac{\partial \boldsymbol{m}_k}{\partial \boldsymbol{x}_j}|_c \beta_{ijk} + \delta\varepsilon \end{aligned} \tag{3.40}$$

Note the last term $\delta\varepsilon$ cancels with the dynamical energy. The second part is from the perturbed Hamiltonian by magnetization gradients,

$$\left\langle W_0|\hat{H}'_{\boldsymbol{m}}|W_0\right\rangle = -\frac{\partial \boldsymbol{m}}{\partial \boldsymbol{x}}|_c \cdot t_{\boldsymbol{pm}}, \tag{3.41}$$

where $t_{\boldsymbol{pm}}$ is the spin dipole associated with the wavepacket,

$$t_{\boldsymbol{pm}} = -Im\left[\langle\frac{\partial u_0}{\partial \boldsymbol{p}}|\cdot(\varepsilon_0 - \hat{H}_c)|\frac{\partial u_0}{\partial \boldsymbol{m}}\rangle\right]. \tag{3.42}$$

The above result is similar to the orbital magnetization of wavepackets by replacing $\boldsymbol{m} \to \boldsymbol{p}$. Note the perturbed Hamiltonian by electric fields does not have the linear order correction, because $\left\langle W|\hat{\boldsymbol{x}} - \boldsymbol{x}_c|W\right\rangle = 0$. The third part is the mixed effect of the magnetization gradients and electric fields, which has two terms:

$$\begin{aligned}
&\left\langle W_{\boldsymbol{E}}|H'_{\boldsymbol{m}}|W_0\right\rangle + c.c. \\
=\ & \sum_{n\neq 0}\int [d\boldsymbol{p}][d\boldsymbol{p}_1]\cdot C^*_{\boldsymbol{E},n}(\boldsymbol{p})H_{\boldsymbol{m},n0}(\boldsymbol{p},\boldsymbol{p}_1)\cdot C_0(\boldsymbol{p}_1) \\
=\ & \sum_{n\neq 0}\int [d\boldsymbol{p}]\cdot C^*_{\boldsymbol{m},n}(\boldsymbol{p})(\varepsilon_0-\varepsilon_n)C_{\boldsymbol{E},n}(\boldsymbol{p}) + C^*_{\boldsymbol{E},n}(\boldsymbol{p})C_0\cdot v_0\frac{\partial \boldsymbol{m}}{\partial \boldsymbol{x}}\big|_c \boldsymbol{A}^m_{n0} + c.c. \\
=\ & E_i\frac{\partial \boldsymbol{m}_{\boldsymbol{k}}}{\partial \boldsymbol{x}_{\boldsymbol{j}}}|_c(\beta_{ijk} + v_{0,j}\gamma_{ik}),
\end{aligned} \tag{3.43}$$

and

$$\begin{aligned}
&\left\langle W_{\boldsymbol{m}}|H'_{\boldsymbol{E}}|W_0\right\rangle + c.c. \\
=\ & \sum_{n\neq 0}\int [d\boldsymbol{p}][d\boldsymbol{p}_1]\cdot C^*_{\boldsymbol{m},n}(\boldsymbol{p})H_{\boldsymbol{E},n0}(\boldsymbol{p},\boldsymbol{p}_1)\cdot C_0(\boldsymbol{p}_1) + c.c \\
=\ & \sum_{n\neq 0}\int [d\boldsymbol{p}]\cdot C^*_{\boldsymbol{m},n}(\boldsymbol{p})(\varepsilon_0-\varepsilon_n)C_{\boldsymbol{E},n}(\boldsymbol{p}) + c.c. \\
=\ & \boldsymbol{E}_i\frac{\partial \boldsymbol{m}_{\boldsymbol{k}}}{\partial \boldsymbol{x}_{\boldsymbol{j}}}|_c\beta_{ijk}.
\end{aligned} \tag{3.44}$$

Note the electric field-induced spin dipole is,

$$\left\langle W_{\boldsymbol{E}}|\hat{\boldsymbol{\sigma}}_k(\hat{\boldsymbol{x}}-\boldsymbol{x}_c)_j|W_0\right\rangle + c.c. = -\boldsymbol{E}_i(\beta_{ijk}+v_{0,j}\gamma_{ik}),$$

and the magnetization gradient-induced polarization is,

$$\left\langle W_{\boldsymbol{m}}|-(\hat{\boldsymbol{x}}-\boldsymbol{x}_c)_i|W_0\right\rangle + c.c. = -\frac{\partial \boldsymbol{m_k}}{\partial \boldsymbol{x_j}}|_c\beta_{ijk}.$$

Combing the Eq. (3.39),Eq. (3.40),Eq. (3.41),Eq. (3.44), the final expression of wavepacket energy is

$$\tilde{\varepsilon} = \varepsilon_0 - \frac{\partial \boldsymbol{m}}{\partial \boldsymbol{x}}|_c \cdot t_{\boldsymbol{pm}} - \boldsymbol{E}_i\frac{\partial \boldsymbol{m}_k}{\partial \boldsymbol{x}_j}|_c\chi_{ijk}, \tag{3.45}$$

where the second-order correction is,

$$\chi_{ijk} \;=\; -\beta_{ijk} - v_{0,j}\gamma_{ik}. \tag{3.46}$$

3.3.5 Effective Lagrangian of Wavepacket

To obtain the influence of electric fields and inhomogeneity on magnetization dynamics, the wavepacket Lagrangian should be derived to the mixed order of electric ands magnetization gradients. Expressing in terms of the center position and center momentum, we have the wavepcket Lagrangian,

$$\mathcal{L} = \dot{\boldsymbol{r}}\boldsymbol{p} + \dot{\boldsymbol{p}}\cdot\tilde{\boldsymbol{a}}_0 + \frac{d\boldsymbol{m}}{dt}\cdot\tilde{\boldsymbol{a}}^m - \tilde{\varepsilon}, \tag{3.47}$$

where the total derivative $d\boldsymbol{m}/dt = \partial_t\boldsymbol{m} + \dot{\boldsymbol{x}}\cdot\partial\boldsymbol{m}/\partial\boldsymbol{x}$, $\tilde{\boldsymbol{a}}_0$ and $\tilde{\boldsymbol{a}}_m$ are the perturbed Berry connections,

$$\begin{aligned}
\tilde{\boldsymbol{a}}_{0,i} &= \boldsymbol{a}_{0,i} + \boldsymbol{E}_j\alpha_{ij} + \frac{\partial \boldsymbol{m}_k}{\partial \boldsymbol{x}_j}\beta_{ijk}, \\
\tilde{\boldsymbol{a}}_{m,i} &= \boldsymbol{a}_{m,i} + \boldsymbol{E}_j\gamma_{ij} + \frac{\partial \boldsymbol{m}_k}{\partial \boldsymbol{x}_j}\eta_{ijk}.
\end{aligned} \tag{3.48}$$

The correction of $\tilde{\boldsymbol{a}}_0$ represents the positional shift of the wavepacket center in the presence of electric fields and magnetization gradients, with the response coefficients α and β. Similarly, the correction of $\tilde{\boldsymbol{a}}_m$ represents the spin variation of wavepackets, with coefficients γ and η. The energy of the wavepacket to the mixed order is,

$$\tilde{\varepsilon} = \varepsilon_0 - \frac{\partial \boldsymbol{m}}{\partial \boldsymbol{x}}|_c \cdot t_{\boldsymbol{pm}} - \boldsymbol{E}_i \frac{\partial \boldsymbol{m}_k}{\partial \boldsymbol{x}_j}|_c \chi_{ijk}. \tag{3.49}$$

Stimulating by the expression of the orbital magnetization, the coefficient $t_{\boldsymbol{pm}}$ is interpreted as the spin dipole density associated with the wavepacket, and $\chi_{ijk} = -\beta_{ijk} - v_{0,j}\gamma_{ki}$ is the field-response coefficient.

The Berry connection is derived to the linear order while the Berry phase effect in the Lagrangian is in the second order. Finally, we mention that the form of the wavepacket Lagrangian is universal even in higher-order theories, where the Berry connections and the wavepacket energy with proper corrections should be used.

3.3.6 Dynamical Equations

According to the Lagrangian principle, the equations of motion for the wavepackets are derived,

$$\begin{aligned} \dot{\boldsymbol{p}} &= -\frac{\partial \tilde{\varepsilon}}{\partial \boldsymbol{x}} + \tilde{\Omega}_{\boldsymbol{xp}} \cdot \dot{\boldsymbol{p}} + \tilde{\Omega}_{\boldsymbol{xx}} \cdot \dot{\boldsymbol{x}} + \tilde{\Omega}_{\boldsymbol{xm}} \cdot \dot{\boldsymbol{m}} - \boldsymbol{E}, \\ \dot{\boldsymbol{x}} &= \frac{\partial \tilde{\varepsilon}}{\partial \boldsymbol{p}} - \tilde{\Omega}_{\boldsymbol{pp}} \cdot \dot{\boldsymbol{p}} - \tilde{\Omega}_{\boldsymbol{px}} \cdot \dot{\boldsymbol{x}} - \tilde{\Omega}_{\boldsymbol{pm}} \cdot \dot{\boldsymbol{m}}. \end{aligned} \tag{3.50}$$

The above equations shares the same structure as the first-order wavepacket theory. The Berry curvatures are defined with the corrected Berry connections,

for example, $\tilde{\Omega}_{\boldsymbol{xp}} = \partial_{\boldsymbol{x}}\tilde{\boldsymbol{a}}_0 - \partial_{\boldsymbol{p}}\tilde{\boldsymbol{a}}_{\boldsymbol{x}}$, and the derivative in $\boldsymbol{x}$ is through $\boldsymbol{m}$ with $\frac{\partial}{\partial \boldsymbol{x}} = \frac{\partial \boldsymbol{m}}{\partial \boldsymbol{x}}\frac{\partial}{\partial \boldsymbol{m}}$, $\tilde{\boldsymbol{a}}_{\boldsymbol{x}} = \frac{\partial \boldsymbol{m}}{\partial \boldsymbol{x}}\tilde{\boldsymbol{a}}_{\boldsymbol{m}}$.

The influences of magnetization motion on the electrons are from two aspects: the electric motive force term in the $\dot{\boldsymbol{p}}$ equation [66] and the charge pumping term in the $\dot{\boldsymbol{x}}$ equation. The dynamics of magnetization itself is assumed with the following Lagrangian,

$$\mathcal{L}_{self} = \boldsymbol{A}_s^m \cdot \dot{\boldsymbol{m}} - G_s, \tag{3.51}$$

where $\boldsymbol{A}_s^m$ is the Berry connection and G_s is the free energy. The subscript s means they are from the magnetization electrons, instead of the electrons we are interested. With the contribution from wavepackets, the total Lagrangian is $\mathcal{L}_{total} = \sum_{wp}\mathcal{L}_{wp} + \mathcal{L}_{self}$. The equation of motion is obtained according to the Lagrangian principle for fields,

$$\dot{\boldsymbol{m}}\Omega_{\boldsymbol{mm},s} + \frac{\partial G_s}{\partial \boldsymbol{m}} = \boldsymbol{h} \tag{3.52}$$

where $\Omega_{\boldsymbol{mm},s} = \nabla_{\boldsymbol{m}} \times \boldsymbol{A}_s^m$ is the Berry curvature of magnetization itself, and the electronic contribution to the total effective $\boldsymbol{H}$ fields is,

$$\begin{aligned} \boldsymbol{h} = & - \int [d\boldsymbol{p}] Df(\frac{\partial \tilde{\varepsilon}}{\partial \boldsymbol{m}} - \tilde{\Omega}_{\boldsymbol{mx}}\dot{\boldsymbol{x}} - \tilde{\Omega}_{\boldsymbol{mp}} \cdot \dot{\boldsymbol{p}} - \tilde{\Omega}_{\boldsymbol{mm}} \cdot \dot{\boldsymbol{m}}) \\ & - \nabla_{\boldsymbol{x}} \cdot \int [d\boldsymbol{p}] Df(\boldsymbol{t}_{\boldsymbol{pm}} + \boldsymbol{E} \cdot \boldsymbol{\chi} + \dot{\boldsymbol{p}} \cdot \boldsymbol{\beta} + \frac{d\boldsymbol{m}}{dt} \cdot \boldsymbol{\eta}). \end{aligned} \tag{3.53}$$

where $[d\boldsymbol{p}] = d^3p/(2\pi)^3$ and the integral is over the Brillouin zone, $D = 1 + Tr\Omega_{\boldsymbol{kx}}$ is the modified density of states and f is the distribution function of electron wave packets.

Before the wavepacket dynamics is substituted into Eq. (3.53), we make the following comments. First, assuming the *sd* coupling between the electron spin and local magnetization, the electronic influences on magnetization should be via the electronic spin in terms of exchange field. The semiclassical result, the $\boldsymbol{h}$ field, is understood as the *wavepacket representation* of the exchange field from spin (or just called spin for simplicity). From Eq. (3.53). The origin of the total exchange field $\boldsymbol{h}$ has two sources:

1. the energy gradients and Faraday $\boldsymbol{h}$ fields,

2. the spatial gradient of the spin dipole of wavepackets.

Second, the result can be generalized to calculate the wavepacket representation of any physical quantity $\hat{\boldsymbol{O}}$. The order parameter $\boldsymbol{m}$ is replaced by the coupling coefficient Θ in the Hamiltonian, $\hat{H} = \hat{H}_c(\hat{\boldsymbol{O}}) - \boldsymbol{\Theta} \cdot \hat{\boldsymbol{O}}$. For example, the electronic velocity can be obtained by coupling the electrons with the electromagnetic field $(\phi, \boldsymbol{A})$.

Third, the above equation applies to both equilibrium and non-equilibrium electrons, since no assumption of wavepacket distribution is made in the derivation. (f is still assumed to be independent of the evolution history.) The Boltzmann equation is used to model the non-equilibrium electrons with distribution deviation,

$$\delta f = -\tau \frac{\partial f_0(\tilde{\varepsilon})}{\partial \tilde{\varepsilon}} \cdot (\dot{\boldsymbol{p}} \frac{\partial \tilde{\varepsilon}}{\partial \boldsymbol{p}} + \dot{\boldsymbol{x}} \frac{\partial \tilde{\varepsilon}}{\partial \boldsymbol{x}} + \dot{\boldsymbol{m}} \frac{\partial \tilde{\varepsilon}}{\partial \boldsymbol{m}}), \tag{3.54}$$

where τ is the relaxation time. More careful discussions on external effects such as positional shift and side jump can be included, but is not the prime of this work.

3.4 Electronic Contribution to the Effective H Fields

In the following, we focus on the electronic contribution to magnetization dynamics in terms of the effective $\boldsymbol{H}$ fields, in the absence and presence of electric fields. The intrinsic and extrinsic part are distinguished by the dependence on relaxation time and discussed in the first and second section, respectively. The third sectio

3.4.1 DMI in Equilibrium and Non-equilibrium

Substituting the wavepacket dynamical equations and distribution in Eq. (3.4), the $\boldsymbol{h}$ field is expressed as a function of the electric fields and magnetization gradients. We first consider the intrinsic effects, which to the mixed order reads,

$$\begin{aligned} \boldsymbol{h} &= -\nabla_{\boldsymbol{x}}\boldsymbol{T}_{\boldsymbol{pm}} - \partial_{\boldsymbol{m}}G \\ &+ e\boldsymbol{E}\cdot\int[d\boldsymbol{p}]\widetilde{\Omega}_{\boldsymbol{pm}}f_0(\widetilde{\varepsilon}) \\ &+ e\boldsymbol{E}\cdot\int[d\boldsymbol{p}]f_0[\Omega_{\boldsymbol{p}[\boldsymbol{p}}\Omega_{\boldsymbol{x}]\boldsymbol{m}} - \Omega_{\boldsymbol{p}[\boldsymbol{x}}\Omega_{\boldsymbol{p}]\boldsymbol{m}} + \Omega_{\boldsymbol{pm}}\Omega_{[\boldsymbol{px}]}]. \end{aligned} \tag{3.55}$$

where $f_0 = f_0(\varepsilon_0)$. The first term in the first line is from the spin dipole density of electrons, the spatial gradient of which contributes to the effective

fields. The spin dipole density includes the equilibrium part $\boldsymbol{T}^{eq}_{\boldsymbol{pm}}$, and the non-equilibrium part in the presence of electric field $\boldsymbol{T}^{E}_{\boldsymbol{pm}}$. First, take $\boldsymbol{E} = 0$ and we have the spin dipole in equilibrium,

$$\boldsymbol{T}^{eq}_{\boldsymbol{pm}} = \int [d\boldsymbol{p}](f_0 t_{\boldsymbol{pm}} - g_0 \Omega_{\boldsymbol{pm}}). \tag{3.56}$$

where the free energy $g_0 = g_0(\varepsilon_0) = -\beta^{-1} ln(1 + \exp[-\beta(\varepsilon_0 - \mu)])$. In the first term, $t_{\boldsymbol{pm}}$ is the field dipole associated with wavepackets. The second term represents the intercell contribution in terms of the mixed Berry curvature. The meaning of each term can be understood in the same way as the Berry-phase formula for the orbital magnetization [62, 15]. Freimuth *et al.* reached the same result for equilibrium DMI [67, 68, 69, 70] using the thermal dynamical definition, which confirms our results extracted from the effective fields. Using a similar method, the antisymmetric part of the spin dipole density, the spin toroidization, is obtained by assuming an inhomogeneity in the Zeeman field [71, 72].

With electric fields, the non-equilibrium part of the spin dipole density is extracted,

$$\boldsymbol{T}^{E}_{\boldsymbol{p}_j \boldsymbol{m}_k} = \kappa_{ijk} \boldsymbol{E}_i, \tag{3.57}$$

with coefficients,

$$\kappa_{ijk} = \int [d\boldsymbol{p}][f_0 \chi_{ijk} - g_0 \delta^{\boldsymbol{E}_i} \Omega_{\boldsymbol{p}_j \boldsymbol{m}_k} - f_0 \beta_{ijk}]. \tag{3.58}$$

Three origins of the non-equilibrium DMI are implied. In the first term, χ_{ijk} represents the spin dipole correction associated with wavepackets. The second

term is from the correction on the mixed Berry curvature by electric fields. These two terms are corrections of the equilibrium expression of DMI. In the third term, β represents the positional shift in the wavepacket center position by magnetization gradients, the reciprocal process of which implies a field-induced spin dipole. Using $\chi_{ijk} = -\beta_{ijk} - v_{0,j}\gamma_{ki}$, we have,

$$\begin{aligned}\kappa_{ijk} &= \int [d\boldsymbol{p}][-f_0\beta_{ijk} - f_0 v_{0,j}\gamma_{ki} - g_0(\frac{\partial\gamma_{ki}}{\partial \boldsymbol{p}_j} - \frac{\partial\alpha_{ji}}{\partial \boldsymbol{m}_k}) - f_0\beta_{ijk}] \\ &= \int [d\boldsymbol{p}][-2f_0\beta_{ijk} + g_0\frac{\partial\alpha_{ji}}{\partial \boldsymbol{m}_k}]. \end{aligned} \tag{3.59}$$

In the wavepacket formulation, the β term is related to the internal structure of wavepacket and should be understood as an intracell contribution. This expression is ready for calculation with Density Functional Theory and tight-binding model. Hua *et al.* studied the field-induced spin on the surface of magnetic insulators [73], which is from the spin dipole induced by electric fields.

The spin dipole contributes to the effective fields in an antisymmetric form of $\boldsymbol{x}$ and $\boldsymbol{m}$. Indeed, the antisymmetric counterpart $-\partial_{\boldsymbol{m}} G_0$ can be found in the second term of the first line, with the equilibrium free energy due to inhomogeneity $G_0 = -\boldsymbol{T}^{eq}_{\boldsymbol{pm}}\partial_{\boldsymbol{x}}\boldsymbol{m}$. However, for the non-equilibrium spin dipole, the rest of the second term is not complete to make an antisymmetric form of $\boldsymbol{T}^{E}_{\boldsymbol{p}_j\boldsymbol{m}_k}$,

$$-\frac{\partial}{\partial \boldsymbol{m}}(G - G_0) = -\frac{\partial}{\partial \boldsymbol{m}} \cdot \int [d\boldsymbol{p}][f_0\chi_{ijk} - g_0\delta^{\boldsymbol{E}_i}\Omega_{\boldsymbol{p}_j\boldsymbol{m}_k}]\frac{\partial \boldsymbol{m}_k}{\partial \boldsymbol{x}_j}\boldsymbol{E}_i. \tag{3.60}$$

In fact, the missing term, $-\frac{\partial}{\partial \boldsymbol{m}}\cdot\int [d\boldsymbol{p}] f_0\beta_{ijk}\frac{\partial \boldsymbol{m}_k}{\partial \boldsymbol{x}_j}\boldsymbol{E}_i$, is recovered from the second line in Eq. (3.55): the effective fields reciprocal to the charge-pumping current.

The completeness of the antisymmetric part confirms that T_{km} is the spin dipole of electrons.

The second and third line in the effective fields are reciprocal to the charge-pumping current. Heuristically these two are the reaction force on magnetization when the adiabatic current is pumped by magnetization motion in the presence of electric field. The Onsager relation of the charge-pumping current and the effective fields is,

$$\boldsymbol{j}_p \cdot \boldsymbol{E} = \boldsymbol{h}_p \cdot \dot{\boldsymbol{m}}. \tag{3.61}$$

The L.H.S is the power density representing the electric work on the charge-pumping current $\boldsymbol{j}_p$. The R.H.S is the energy variation of the electrons. By expanding the second line and doing partial integral, the effective fields reciprocal to the current is written explicitly,

$$\boldsymbol{h}_p = e\boldsymbol{E} \cdot \int [d\boldsymbol{p}] f_0 (\Omega_{\boldsymbol{pm}} + \Omega^2_{\boldsymbol{p[xp]m}}) + \boldsymbol{\phi}_{ijk} E_i \frac{\partial m_k}{\partial x_j} - \frac{\partial}{\partial \boldsymbol{m}} \cdot \int [d\boldsymbol{p}] f_0 \beta_{ijk} \frac{\partial \boldsymbol{m}_k}{\partial \boldsymbol{x}_j} \boldsymbol{E}_i, \tag{3.62}$$

where $\Omega^2_{\boldsymbol{pxpm}}$ stands for the second Chern form, and

$$\boldsymbol{\phi}_{ijk} = \int [d\boldsymbol{p}] f_0' (-v_{0,i} \boldsymbol{\eta}_{jk} + v_{\boldsymbol{m}} \beta_{ijk} - t_{p_j m_k} \Omega_{p_i \boldsymbol{m}}), \tag{3.63}$$

where the vector $(\boldsymbol{\eta}_{jk})_i = \eta_{ijk}$. The $\Omega_{\boldsymbol{pm}}$ term already exists in the uniform magnetization. In the following, we comment on the remaining three terms.

First, the second Chern form are antisymmetric in the four indexes, implying that: The spatial dimension of system should be at least two and the dimension of electronic Hamiltonian should be at least three to obtain

a nonzero second Chern form. Therefore, it does not appear in two-band ferromagnets. In multi-band ferromagnets, for example, VSe2 monolayer, a two-dimensional Vander Waals ferromagnets [74, 75, 76, 77], the second Chern form contribution to the effective fields is expected to be important.

Second, the $\boldsymbol{\phi}$ term is an intrinsic Fermi surface contribution, which is important for metals and does not depend on impurity properties. The expression of $\boldsymbol{\phi}$ contains the mixture of intercell and intracell contributions, and its meaning needs further exploration. The last term is from the polarization induced by the magnetization inhomogeneity, which couples with electric fields and gives an energy gradient term.

Together with the free energy G, the enthalpy of the electronic system is extracted,

$$\begin{aligned} F &= G + \int [d\boldsymbol{p}] f_0 \beta_{ijk} \frac{\partial \boldsymbol{m}_k}{\partial \boldsymbol{x}_j} \boldsymbol{E}_i, \\ &= \int [d\boldsymbol{p}](1 + \tilde{\Omega}_{\boldsymbol{px}}) g_0(\tilde{\varepsilon}) + f_0 \beta_{ijk} \frac{\partial \boldsymbol{m}_k}{\partial \boldsymbol{x}_j} \boldsymbol{E}_i \\ &= \int [d\boldsymbol{p}](1 + \tilde{\Omega}_{\boldsymbol{px}}) g_0(\tilde{\varepsilon}'), \end{aligned} \tag{3.64}$$

where the energy for enthalpy definition is,

$$\tilde{\varepsilon}' = \varepsilon_0 - \frac{\partial \boldsymbol{m}}{\partial \boldsymbol{x}}|_c \cdot t_{\boldsymbol{pm}} - \boldsymbol{E}_i \frac{\partial \boldsymbol{m}_k}{\partial \boldsymbol{x}_j}|_c (\chi_{ijk} - \beta_{ijk}). \tag{3.65}$$

In the end, the effective fields are represented by the state function terms, the Berry curvature terms and the Fermi surface terms,

$$\boldsymbol{h} = \partial_{\boldsymbol{x}} \frac{\partial F}{\partial \partial_x m} - \partial_{\boldsymbol{m}} F + e\boldsymbol{E} \cdot \int [d\boldsymbol{p}] f_0 (\Omega_{\boldsymbol{pm}} + \Omega^2_{\boldsymbol{p}[\boldsymbol{xp}]\boldsymbol{m}}) + \boldsymbol{\phi}_{ijk} E_i \frac{\partial m_k}{\partial x_j}. \tag{3.66}$$

In metalic ferromagnets, external contributions to the effective fields are equally important as the intrinsic counterpart. According to Eq. (3.53), the non-equilibrium electrons due to relaxations contribute to the spin dipole density as well. Using the Boltzmann equation, the spin dipole associated with wavepacket of the non-equilibrium electrons is obtained,

$$\boldsymbol{T}^{ex}_{\boldsymbol{pm}} = \int [d\boldsymbol{p}] \boldsymbol{t}_{\boldsymbol{pm}} (e\boldsymbol{E}\tau \cdot \partial_{\boldsymbol{p}} f_0). \tag{3.67}$$

The relaxation time dependence implies the current-induced nature of the external DMI. In parallel, the current-induced orbital magnetization has been discussed in metallic noncentrosymmetric crystals, also known as the orbital Edelstein effect. Different from the intrinsic spin dipole density, $\boldsymbol{T}^{ex}_{\boldsymbol{pm}}$ does not have an enthalpy counterpart, and hence it cannot be obtained by thermal dynamical approaches.

3.4.2 Thermal Dynamical Relation

At zero termperatures, the enthalpy (density) of insulator in the presence of electric fields is defined as

$$f = u - \mu n - \boldsymbol{E} \cdot \boldsymbol{P}, \tag{3.68}$$

where $u, n, \boldsymbol{P}$ are the internal energy density, particle number density and polarization, respectively, for constant chemical potential μ. The work density by electric fields and magnetization changes the internal energy density as,

$$du = \boldsymbol{E} \cdot d\boldsymbol{P} - \boldsymbol{S} \cdot d\boldsymbol{m}, \tag{3.69}$$

where $\boldsymbol{S}$ denotes the spin density (The exchange constant $J = 1$). In the presence of spatial gradient, the spin dipole density $\boldsymbol{T}$ should be considered. Then the variation of the internal energy density is,

$$\begin{aligned} du &= \boldsymbol{E} \cdot d\boldsymbol{P} - (\boldsymbol{S} - \frac{\partial \boldsymbol{T}}{\partial \boldsymbol{x}}) \cdot d\boldsymbol{m} \\ &= \boldsymbol{E} \cdot d\boldsymbol{P} - \boldsymbol{S} \cdot d\boldsymbol{m} - \boldsymbol{T} \cdot d\frac{\partial \boldsymbol{m}}{\partial \boldsymbol{x}}, \end{aligned} \tag{3.70}$$

where a total derivative is discarded. As results, the variation of the enthalpy is written as,

$$df = -nd\mu - \boldsymbol{S} \cdot d\boldsymbol{m} - \boldsymbol{T}_{\boldsymbol{pm}} \cdot d\frac{\partial \boldsymbol{m}}{\partial \boldsymbol{x}} - \boldsymbol{P} \cdot d\boldsymbol{E}. \tag{3.71}$$

It implies that the enthalpy is a function of $\mu, \boldsymbol{m}, \partial \boldsymbol{m}/\partial \boldsymbol{x}, \boldsymbol{E}$. Therefore, we have the Maxwell relation,

$$\frac{\partial \boldsymbol{T}_{\boldsymbol{p}_j \boldsymbol{m}_k}}{\partial \mu} = \frac{\partial n}{\partial \frac{\partial \boldsymbol{m}_k}{\partial \boldsymbol{x}_j}}. \tag{3.72}$$

Because the particle number variation is proportional to the charge density, we have $\delta n = \frac{\partial \boldsymbol{P}_j}{\partial \boldsymbol{x}_j}$ and

$$\frac{\partial \boldsymbol{T}_{\boldsymbol{p}_j \boldsymbol{m}_k}}{\partial \mu} = \frac{\partial \boldsymbol{P}_j}{\partial \boldsymbol{m}_k}. \tag{3.73}$$

Our results on the spin dipole density induced by electric fields satisfies the above Maxwell relation,

$$\frac{\partial \boldsymbol{T}^{\boldsymbol{E}_i}_{\boldsymbol{p}_j \boldsymbol{m}_k}}{\partial \mu} = \int [d\boldsymbol{p}] \frac{\partial \alpha_{ji}}{\partial \boldsymbol{m}_k} \boldsymbol{E}_i = \frac{\partial \boldsymbol{P}^{\boldsymbol{E}_i}_j}{\partial \boldsymbol{m}_k}, \tag{3.74}$$

where the polarization change by electric field is used [78],

$$\delta \boldsymbol{P}^{\boldsymbol{E}_i}_j = \alpha_{ji} \boldsymbol{E}_i. \tag{3.75}$$

3.4.3 Gyromagnetic Ratio and Damping Corrections

The $\dot{\boldsymbol{m}}$ dependent terms in the effective fields represent the correction on the gyromagnetic ratio and damping. First, the Berry curvature is corrected by electric fields as,

$$\tilde{\Omega}_{\boldsymbol{mm}} = \Omega_{\boldsymbol{mm}} + \partial_{\boldsymbol{m}} \times \gamma_{j\boldsymbol{m}} E_j. \tag{3.76}$$

By doing partial integral, the Berry curvature correction turns out to be a Fermi surface contribution, $\delta\bar{\Omega}_{\boldsymbol{mm}} = -\int [d\boldsymbol{p}] f_0' v_{\boldsymbol{m}} \times \gamma_{j\boldsymbol{m}} E_j$. The correction should be important in metals with clear Fermi surface, and the antisymmetric coefficient implies a field-induced gyromagnetic ratio in metallic magnets. Notably, the Fermi surface contribution is intrinsic and independent of the relaxation, in comparison with the extrinsic contribution derived from the Boltzmann equation.

Second, the magnetization motion induces a geometric term in the $\boldsymbol{h}$ field in the second Chern form,

$$\boldsymbol{h_d} = \dot{\boldsymbol{m}} \cdot \int [dp] f_0 \Omega^2_{\boldsymbol{m}[\boldsymbol{xp}]\boldsymbol{m}}, \tag{3.77}$$

where subscript d means *dynamical*. This term vanishes when the inhomogeneity is from the magnetization, because the second Chern form is antisymmetric in the four indexes. It implies that an inhomogeneity from other sources generally influences the gyromagnetic ratio. Finally, the magnetization motion induces a spin dipole, $T^D_{km} = \dot{M}\eta$, which contributes to the gyromagnetic ratio and damping in general.

Table 3.1: Comparison of the magnetization dynamics for the uniform and non-uniform ferromagnetic insulators.

Role in LLG	The uniform case	The non-uniform case
State function	G	$G - T_{\boldsymbol{pm}} \cdot \nabla_{\boldsymbol{x}} \boldsymbol{m}$
Driven force	$e\boldsymbol{E} \cdot \Omega_{\boldsymbol{pm}}$	$e\boldsymbol{E} \cdot [\Omega_{\boldsymbol{pm}} + \Omega^2_{\boldsymbol{p[xp]m}}]$
Gyromagnetic ratio	$\Omega_{\boldsymbol{mm}}$	$\Omega_{\boldsymbol{mm}} + \Omega^2_{\boldsymbol{m[xp]m}}$

Before we end the discussion on the semiclassical framework, we summarize the electronic contribution to magnetization dynamics in uniform and non-uniform magnetic materials in terms the effective $\boldsymbol{h}$ fields in Table. (3.1). For simplicity, we are considering an ferromagnetic insulator.

3.5 Numerical Results on Transition Metal Dichalcogenide materials

In the following, we use the Transition Metal Dichalcogenide (TMD) materials, for example, WTe2 for its large spin-orbital coupling [79], to show the equilibrium and non-equilibrium spin dipole and spin density. We focus on insulators and set zero temperatures. The electrons couple with a 2D ferromagnet by exchange interaction in the following Hamiltonian,

$$\hat{H} = \hat{H}_0 + J\hat{\boldsymbol{\sigma}} \cdot \boldsymbol{m}, \tag{3.78}$$

where the second term is the exchange coupling between the electron spin and the magnetization of ferromagnets. H_0 is the six-band electronic Hamiltonian,

$$\hat{H}_0 = \begin{pmatrix} \hat{H}^{NN} + \frac{\lambda}{2}\hat{L}_z & 0 \\ 0 & \hat{H}^{NN} - \frac{\lambda}{2}\hat{L}_z \end{pmatrix}, \tag{3.79}$$

with the nearest neighboring hopping terms,

$$\hat{H}^{NN} = \begin{pmatrix} h_0 & h_1 & h_2 \\ h_1^* & h_{11} & h_{12} \\ h_2^* & h_{12}^* & h_{22} \end{pmatrix}. \tag{3.80}$$

The expression of the h's can be found in reference [80].

3.5.1 Spin Density: Geometric Contribution

The geometric contribution to spin density is,

$$\boldsymbol{h}_k^t = e\boldsymbol{E} \cdot \int [d\boldsymbol{p}] f_0 (\Omega_{\boldsymbol{pm}} + \Omega^2_{\boldsymbol{p}[\boldsymbol{xp}]\boldsymbol{m}}). \tag{3.81}$$

We consider a domain wall with easy axis in the z direction. It is described by the polar angle θ and azimuthal angle ϕ,

$$\theta = \tan^{-1}\frac{y}{w_0} + \frac{\pi}{2}, \tag{3.82}$$

$$\phi = 0, \text{ Bloch type} \tag{3.83}$$

where w_0 is the domain wall width. The Bloch type domain wall is shown in Fig. 3.4. Under electric fields in the x direction, the induced spin is plotted in components in Fig. 3.5. With the lowest two bands filled, the first Chern form contribution vanishes. The dominant component, $\delta \boldsymbol{s}_y$, is antisymmetric on the two sides of the domain wall center. Thus the torque exerted on magnetization

$\delta\boldsymbol{\tau} \sim -\boldsymbol{m} \times \delta\boldsymbol{s}$ is in the x direction on both sides, increasing the width of the domain wall. For the Neel type domain wall, similar analysis shows that the width of domain wall is also increased in the presence of electric fields. See Fig. 3.6 and Fig. 3.5.

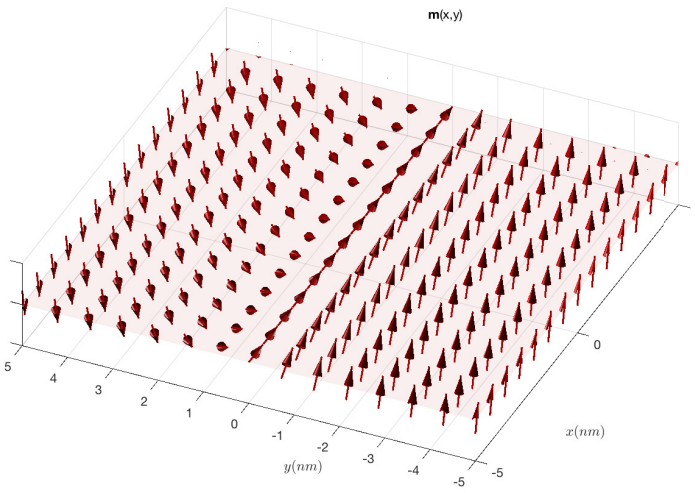

Figure 3.4: (Color online) The Bloch type domain wall with easy axis z. Parameters: $w_0 = 10$ nm.

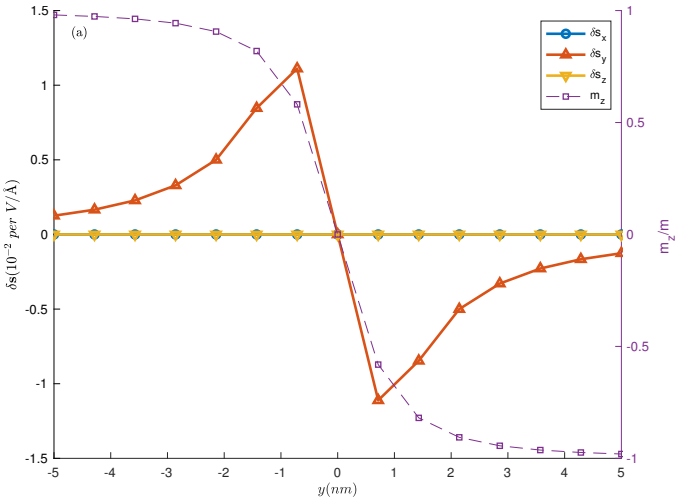

Figure 3.5: (Color online) The induced spin in a unit cell from the second Chern form, $\Omega^2_{\boldsymbol{p}[\boldsymbol{xp}]\boldsymbol{m}}$ for the Bloch type domain wall.

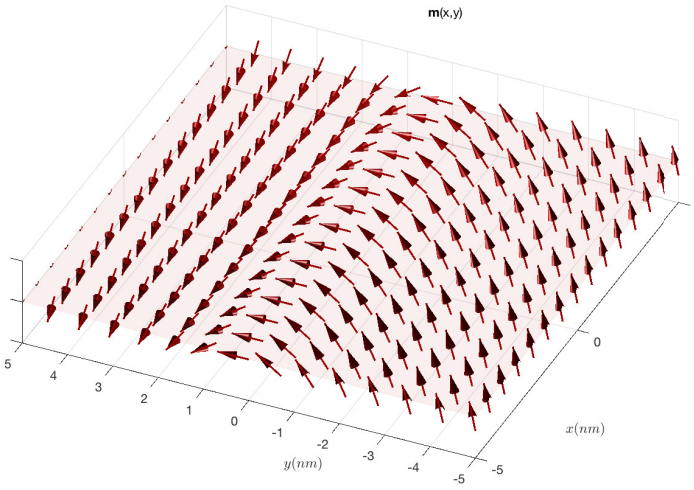

Figure 3.6: (Color online) The Neel type domain wall with easy axis z. Parameters: $w_0 = 10$ nm.

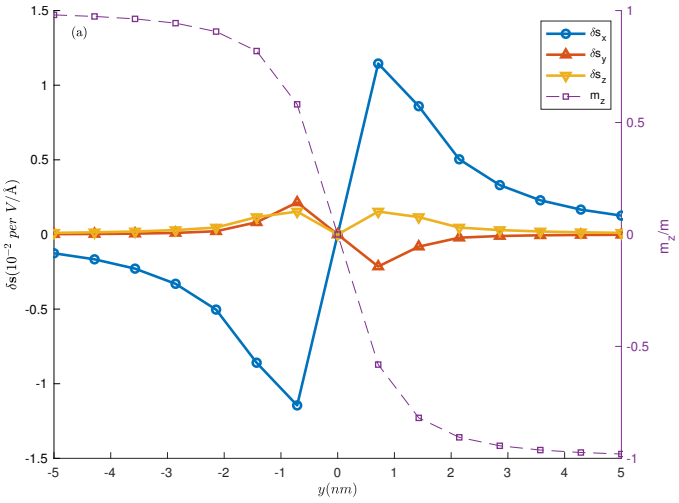

Figure 3.7: (Color online) The induced spin in a unit cell from the second Chern form, $\Omega^2_{\boldsymbol{p[xp]m}}$ for the Neel type domain wall.

The electric work is an topological invariance, considering the work density along the x direction ,

$$\begin{aligned}\frac{W}{dx} &= \int j_p \cdot E \cdot dydt \\ &= \int dp_x dp_y d^2S \cdot eE[\Omega_{p_x p_y}\Omega_{m'm} - \Omega_{p_x m'}\Omega_{p_y m} + \Omega_{p_x m}\Omega_{p_y m'}] \\ &= eEC_2, \end{aligned} \tag{3.84}$$

where C_2 is the second Chern number. The trajectory of magnetization of the domain wall should cover the whole magnetization sphere, which requires that the magnetization of the domain wall should rotate 2π around the z axis. The Neel type and Bloch type domain wall are one of the stages during the rotation. The work density along the x direction can be evaluated as

$$\frac{W}{dx} \sim \delta \boldsymbol{m} \cdot \delta \boldsymbol{s} = \delta\phi \hat{z} \times m \cdot \delta s = \delta\phi(m_x \delta s_y - m_y \delta s_x), \tag{3.85}$$

where $\delta\phi$ is the azimuth angle variation. From Fig. 3.5 and 3.7, the x and y components of the induced spin are antisymmetric around the domain wall center, and the x and y components of the magnetization are symmetric. Therefore, the electric work is also antisymmetric around the the domain wall center, and the total is zero, $C_2 = 0$.

3.5.2 Spin Density: Spin Dipole Contribution

We first evaluate the coefficient of spin dipole response for insulators at zero temperatures,

$$\begin{aligned} \kappa_{ijk} &= \int [d\boldsymbol{p}][-2f_0\beta_{ijk} + g_0\frac{\partial\alpha_{ji}}{\partial \boldsymbol{m}_k}], \\ &= \int [d\boldsymbol{p}][-2\beta_{ijk} + (\varepsilon_0 - \mu)\frac{\partial\alpha_{ji}}{\partial \boldsymbol{m}_k}], \\ &= \int [d\boldsymbol{p}][-2\sum_{n\neq 0}\frac{iV^i_{0n}Q^{jk}_{n0} + c.c.}{(\varepsilon_0 - \varepsilon_n)^2} + (\varepsilon_0 - \mu)\frac{\partial\alpha_{ji}}{\partial \boldsymbol{m}_k}], \end{aligned} \tag{3.86}$$

with the field-induced positional shift, $\alpha_{ji} = e\cdot\sum_{n\neq 0}\frac{V^j_{0n}V^i_{n0}}{(\varepsilon_0-\varepsilon_n)^3} + c.c$, and inter-band spin dipole elements, $Q^{jk}_{n0} = v_{0,j}A^{m,k}_{n0} + \sum_{n_2\neq 0}\sigma^k_{nn_2}A^j_{n_20}$. Then the spin density due to spin dipole is,

$$\boldsymbol{h}^F_k = (\partial_{m_k}\kappa_{ijl} - \partial_{m_l}\kappa_{ijk})E_i\partial_{x_j}m_l. \tag{3.87}$$

The results of numerical simulation show complicated behaviors of the induced spin density in space. One can observe that the magnitudes of the spin density is around 10 times bigger than the geometric contribution. Therefore, the spin dipole contribution should be dominant in the field-induced spin density.

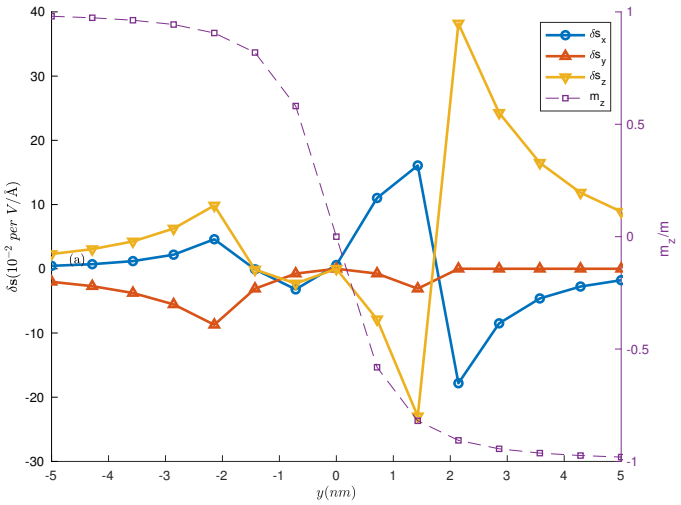

Figure 3.8: (Color online) The induced spin in a unit cell from the spin dipole for the Bloch type domain wall.

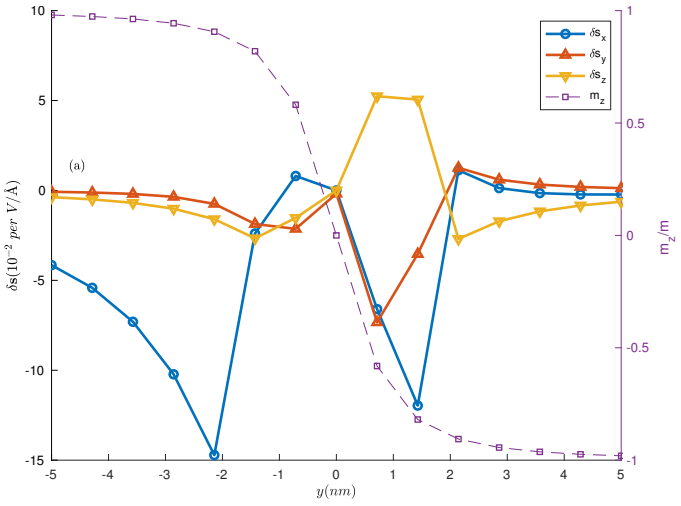

Figure 3.9: (Color online) The induced spin in a unit cell from the spin dipole for the Neel type domain wall.

Because the x and y components of the induced spin are not antisymmetric, the total work density is nonzero at the two stages of the Neel type and Bloch type configuration. This implies that the total energy of the system is changing when the magnetization is rotating around the z axis. However, when the magnetization rotates one full circle, the total energy should not change.

Appendices

Appendix A

Derivation of Magnetization Dynamics

The wavepacket is regarded as a particle that has center momentum k_c and center position r_c. The Lagrangian of wavepacket is

$$\mathcal{L} = \langle W | i\hbar \frac{d}{dt} - \hat{H} | W \rangle,$$

which can be explicitly written as

$$\mathcal{L}(x_c, k_c, \dot{x}_c, \dot{k}_c) = \dot{x}_c(k_c - eA) + \dot{k}_c A_{k_c} + \dot{x}_c A_{x_c} + A_t - (\varepsilon - e\phi).$$

For the many wavepakcets interacting with a magnetization field, $m(x,t)$, the total Lagrangian of the system is

$$\mathcal{L} = \sum_i \mathcal{L}^i = \sum_i L(x_c^i, k_c^i, \dot{x}_c^i, \dot{k}_c^i; [m(x_c^i, t)]),$$

where $[m]$ means functional of field m. Written in term of Lagrangian density, it is

$$\mathcal{L} = \int [dx] \sum_i \delta(x - x_c^i(t)) L(x_c^i, k_c^i, \dot{x}_c^i, \dot{k}_c^i; [m(x,t)]),$$

with the density $\mathcal{L}_d$ is the intergrand. Note that we only replace

$$m(x_c^i, t) \to m(x,t),$$

while the label of electrons, superscript i, is kept in others variables. Therefore quantities below are functions of $k_c^i, m(x,t)$:

$$[A_{k_c^i}, A_x, A_m, A_t, \varepsilon, T^1_{k_c^i m}] \text{ depends on } \big(k_c^i, m(x,t)\big).$$

Now we do the Lagrangian principle for fields $m(x,t)$,

$$\frac{\partial \mathcal{L}_d}{\partial m} = \sum_i \delta\big(x - x_c^i(t)\big) \frac{\partial}{\partial m}[\dot{k}_c^i A_{k_c^i} + \dot{x}_c^i A_x + A_t - \varepsilon],$$

and

$$\frac{\partial \mathcal{L}_d}{\partial(\partial_x m)} = \sum_i \delta\big(x - x_c^i(t)\big)[\dot{x}_c^i A_m + T^1_{k_c^i m}],$$

then

$$\partial_x \frac{\partial \mathcal{L}_d}{\partial(\partial_x m)} = \sum_i \partial_x \delta\big(x - x_c^i(t)\big)[\dot{x}_c^i A_m + T^1_{k_c^i m}] + \sum_i \delta\big(x - x_c^i(t)\big)\partial_x[\dot{x}_c^i A_m + T^1_{k_c^i m}],$$

and

$$\frac{\partial \mathcal{L}_d}{\partial(\partial_t m)} = \sum_i \delta\big(x - x_c^i(t)\big) A_m.$$

Note the operator ∂_t, when $x_c^i(t), k_c^i(t), t$ are present, includes the time derivative through x_c^i, k_c^i, and t directly,

$$\partial_t \to \sum_j (\dot{x}_c^j \partial_{x_c^j} + \dot{k}_c^j \partial_{k_c^j}) + \partial_t.$$

Then,

$$\partial_t \frac{\partial L_d}{\partial(\partial_t m)} = \sum_i \dot{x}_c^i \frac{\partial}{\partial x_c^i} \delta\big(x - x_c^i(t)\big) A_m + \sum_i \delta\big(x - x_c^i(t)\big)[\dot{m}\frac{\partial}{\partial m} A_m + \dot{k}_c^i \frac{\partial}{\partial k_c^i} A_m].$$

Combining these terms, we have

$$\sum_i \delta\big(x - x_c^i(t)\big)(\dot{m}\Omega_{mm} + \dot{x}_c^i \Omega_{xm} + \dot{k}_c^i \Omega_{k_c^i m} + \frac{\partial \varepsilon}{\partial m} + \partial_x T^1_{k_c^i m}) + \sum_i \partial_x \delta\big(x - x_c^i(t)\big) T^1_{k_c^i m} = 0.$$

Note terms in the bracket are function of x, k. The summation is over wavepacket i, which can be written in integral as

$$\sum_{x_c^i(t),k_c^i(t)} => \int [dk_c dx_c] D(x_c, k_c) \cdot f(x_c, k_c),$$

where D is the modified density of states in phase space volume $[dk_c dx_c]$; f is the occupation probability. Doing that gives the following equation of motion

$$\int [dk_c] Df(\dot{m}\Omega_{mm} + \dot{x}\Omega_{xm} + \dot{k}\Omega_{km} + \frac{\partial \varepsilon}{\partial m}) + \partial_x (\int [dk_c] Df \cdot T^1_{km}) = 0.$$

Appendix B

Perturbation Coefficients

To calculate the coefficient C_n, we have to deal with the scattering matrix of position operator $\hat{\boldsymbol{x}}$. Using the periodicity of Bloch states, we have the following scattering elements of perturbation,

$$\begin{aligned} H'_{E,n0}(\boldsymbol{p},\boldsymbol{p}_1) &= e\boldsymbol{E}\cdot\left\langle\psi_{n,\boldsymbol{p}}|(\hat{\boldsymbol{r}}-\boldsymbol{r}_c)|\psi_{0,\boldsymbol{p}_1}\right\rangle \\ &= e\boldsymbol{E}\cdot(i\partial_{\boldsymbol{p}}\delta_{n0}+\boldsymbol{A}_{n0}-\boldsymbol{r}_c\delta_{n0})\delta(\boldsymbol{p}-\boldsymbol{p}_1), \end{aligned} \tag{B.1}$$

and

$$\begin{aligned} H'_{m,n0}(\boldsymbol{p},\boldsymbol{p}_1) &= -\frac{\partial\boldsymbol{m}}{\partial\boldsymbol{r}}\Big|_c\cdot\left\langle\psi_{n,\boldsymbol{p}}|\hat{\boldsymbol{\sigma}}(\hat{\boldsymbol{r}}-\boldsymbol{r}_c)|\psi_{0,\boldsymbol{p}_1}\right\rangle \\ &= -\frac{\partial\boldsymbol{m}}{\partial\boldsymbol{r}}\Big|_c\cdot\sum_{n_1}\boldsymbol{\sigma}_{nn_1}\left[i\partial_{\boldsymbol{p}}\delta_{n_10}+\boldsymbol{A}_{n_10}-\boldsymbol{r}_c\delta_{n_10}\right]\delta(\boldsymbol{p}-\boldsymbol{p}_1). \end{aligned} \tag{B.2}$$

In general, the numerator in C_n has the following form, $\left\langle\psi_{n,\boldsymbol{p}}|H'_s|\psi_{0,\boldsymbol{p}_1}\right\rangle = f(\boldsymbol{p})\partial_{\boldsymbol{p}}\delta(\boldsymbol{p}-\boldsymbol{p}_1)+g(\boldsymbol{p})\delta(\boldsymbol{p}-\boldsymbol{p}_1)$, where f and g are functions of $\boldsymbol{p}$. The first part involves gradient of delta function, $\partial_{\boldsymbol{p}}\delta(\boldsymbol{p}-\boldsymbol{p}_1)$. By doing partial integral

we have, (needs change later, $\boldsymbol{q} \to \boldsymbol{p}$)

$$\begin{aligned} C_n &= \int [d\boldsymbol{p}_1] C_0(\boldsymbol{p}_1) \frac{f(\boldsymbol{p})}{\varepsilon_{0,\boldsymbol{p}_1} - \varepsilon_{n,\boldsymbol{p}}} \partial_{\boldsymbol{p}} \delta(\boldsymbol{p} - \boldsymbol{p}_1) \\ &= \partial_{\boldsymbol{p}} \int [d\boldsymbol{p}_1] \frac{C_0(\boldsymbol{p}_1) f(\boldsymbol{p})}{\varepsilon_{0,\boldsymbol{p}_1} - \varepsilon_{n,\boldsymbol{p}}} \delta(\boldsymbol{p} - \boldsymbol{p}_1) - \int [d\boldsymbol{p}_1] \cdot \partial_{\boldsymbol{p}} \frac{C_0(\boldsymbol{p}_1) f(\boldsymbol{p})}{\varepsilon_{0,\boldsymbol{p}_1} - \varepsilon_{n,\boldsymbol{p}}} \cdot \delta(\boldsymbol{p} - \boldsymbol{p}_1) \\ &= \partial_{\boldsymbol{p}} C_0(\boldsymbol{p}) \frac{f(\boldsymbol{p})}{\varepsilon_{0,\boldsymbol{p}} - \varepsilon_{n,\boldsymbol{p}}} - C_0(\boldsymbol{p}) \frac{f(\boldsymbol{p})}{(\varepsilon_{0,\boldsymbol{p}} - \varepsilon_{n,\boldsymbol{p}})^2} \partial_{\boldsymbol{p}} \varepsilon_{0,\boldsymbol{p}} \end{aligned} \tag{B.3}$$

Thus the partial derivatives are finally on the $\boldsymbol{p}_1$ dependent terms. The first term involves gradient on C_0, which contributes to the horizontal effects in the following. The second term implies the Berry phase effect, as the electron travels in the inhomogeneous environment with velocity $\partial_{\boldsymbol{p}} \varepsilon_{0,\boldsymbol{p}}$. Our perturbation on wavepacket agrees with Yang Gao's construction using the wave equation, where the two terms are obtained based on the time evolution of coefficients, $i\hbar \dot{C}_n \approx \varepsilon_{0,\boldsymbol{p}} C_n$.

By applying the above results, we obtain the coefficients for electric field perturbation and magnetization perturbation in the main text.

Bibliography

[1] Aurelien Manchon. A new moment for berry. *Nature Physics*, 10:340 EP –, 04 2014.

[2] H. Kurebayashi, Jairo Sinova, D. Fang, A. C. Irvine, T. D. Skinner, J. Wunderlich, V. Novák, R. P. Campion, B. L. Gallagher, E. K. Vehstedt, L. P. Zârbo, K. Výborný, A. J. Ferguson, and T. Jungwirth. An antidamping spin-orbit torque originating from the berry curvature. *Nat Nano*, 9(3):211–217, 03 2014.

[3] Junya Shibata, Gen Tatara, and Hiroshi Kohno. A brief review of field- and current-driven domain-wall motion. *Journal of Physics D: Applied Physics*, 44(38):384004, 2011.

[4] A. Manchon, I.M. Miron, T. Jungwirth, J. Sinova, J. Zelezný, A. Thiaville, K. Garello, and P. Gambardella. Current-induced spin-orbit torques in ferromagnetic and antiferromagnetic systems. *arXiv: 1801.09636*, 2018.

[5] Yang Gao, Shengyuan A. Yang, and Qian Niu. Geometrical effects in orbital magnetic susceptibility. *Phys. Rev. B*, 91:214405, Jun 2015.

[6] S. Zhang and Z. Li. Roles of nonequilibrium conduction electrons on the magnetization dynamics of ferromagnets. *Phys. Rev. Lett.*, 93:127204, 2004.

[7] Shufeng Zhang and Steven S.-L. Zhang. Generalization of the landau-lifshitz-gilbert equation for conducting ferromagnets. *Phys. Rev. Lett.*, 102:086601, Feb 2009.

[8] Kjetil M. D. Hals and Arne Brataas. Phenomenology of current-induced spin-orbit torques. *Phys. Rev. B*, 88:085423, Aug 2013.

[9] Ion Garate and A. H. MacDonald. Influence of a transport current on magnetic anisotropy in gyrotropic ferromagnets. *Phys. Rev. B*, 80:134403, Oct 2009.

[10] Ion Garate and M. Franz. Inverse spin-galvanic effect in the interface between a topological insulator and a ferromagnet. *Phys. Rev. Lett.*, 104:146802, Apr 2010.

[11] Frank Freimuth, Stefan Blügel, and Yuriy Mokrousov. Direct and inverse spin-orbit torques. *Phys. Rev. B*, 92:064415, Aug 2015.

[12] Ganesh Sundaram and Qian Niu. Wave-packet dynamics in slowly perturbed crystals: Gradient corrections and berry-phase effects. *Phys. Rev. B*, 59:14915–14925, Jun 1999.

[13] Gerardo Ortiz and Richard M. Martin. Macroscopic polarization as a geometric quantum phase: Many-body formulation. *Phys. Rev. B*, 49:14202–14210, May 1994.

[14] Di Xiao, Junren Shi, and Qian Niu. Berry phase correction to electron density of states in solids. *Phys. Rev. Lett.*, 95:137204, Sep 2005.

[15] Junren Shi, G. Vignale, Di Xiao, and Qian Niu. Quantum theory of orbital magnetization and its generalization to interacting systems. *Phys. Rev. Lett.*, 99:197202, Nov 2007.

[16] L. D. Landau and E. M. Lifshitz. On the theory of the dispersion of magnetic permeability in ferromagnetic bodies. *Phys. Zs. Sowjet.*, 8:153–169, 1935.

[17] Thomas L. Gilbert. A lagrangian formulation of the gyromagnetic equation of the magnetization field. *Phys. Rev.*, 100(1243), 1955.

[18] T. L. Gilbert. A phenomenological theory of damping in ferromagnetic materials. *IEEE Transactions on Magnetics*, 40(6):3443–3449, Nov 2004.

[19] Qian Niu and Leonard Kleinman. Spin-wave dynamics in real crystals. *Phys. Rev. Lett.*, 80:2205–2208, Mar 1998.

[20] Q. Niu, Xindong Wang, L. Kleinman, Wu-Ming Liu, D. M. C. Nicholson, and G. M. Stocks. Adiabatic dynamics of local spin moments in itinerant magnets. *Phys. Rev. Lett.*, 83:207–210, Jul 1999.

[21] Di Xiao, Ming-Che Chang, and Qian Niu. Berry phase effects on electronic properties. *Rev. Mod. Phys.*, 82:1959–2007, Jul 2010.

[22] Bangguo Xiong, Hua Chen, Xiao Li, and Qian Niu. Geometric dynamics of magnetization: Electronic contribution. *arXiv:1709.09513*, 2017.

[23] J. A. C. Bland and B. Heinrich. *Ultrathin Magnetic Structures III: Fundamentals of Nanomagnetism.* SpringerVerlag, New York, 2005.

[24] D.C. Ralph and M.D. Stiles. Spin transfer torques. *Journal of Magnetism and Magnetic Materials*, 320(7):1190 – 1216, 2008.

[25] A. Manchon and S. Zhang. Theory of nonequilibrium intrinsic spin torque in a single nanomagnet. *Phys. Rev. B*, 78:212405, Dec 2008.

[26] D. A. Pesin and A. H. MacDonald. Quantum kinetic theory of current-induced torques in rashba ferromagnets. *Phys. Rev. B*, 86:014416, Jul 2012.

[27] Xuhui Wang and Aurelien Manchon. Diffusive spin dynamics in ferromagnetic thin films with a rashba interaction. *Phys. Rev. Lett.*, 108:117201, Mar 2012.

[28] Frank Freimuth, Stefan Blügel, and Yuriy Mokrousov. Spin-orbit torques in co/pt(111) and mn/w(001) magnetic bilayers from first principles. *Phys. Rev. B*, 90:174423, Nov 2014.

[29] Alexandr Chernyshov, Mason Overby, Xinyu Liu, Jacek K. Furdyna, Yuli Lyanda-Geller, and Leonid P. Rokhinson. Evidence for reversible control of magnetization in a ferromagnetic material by means of spin–orbit magnetic field. *Nature Physics*, 5:656, 08 2009.

[30] A. R. Mellnik, J. S. Lee, A. Richardella, J. L. Grab, P. J. Mintun, M. H. Fischer, A. Vaezi, A. Manchon, E. A. Kim, N. Samarth, and D. C.

Ralph. Spin-transfer torque generated by a topological insulator. *Nature*, 511(7510):449–451, 07 2014.

[31] Yabin Fan, Pramey Upadhyaya, Xufeng Kou, Murong Lang, So Takei, Zhenxing Wang, Jianshi Tang, Liang He, Li-Te Chang, Mohammad Montazeri, Guoqiang Yu, Wanjun Jiang, Tianxiao Nie, Robert N. Schwartz, Yaroslav Tserkovnyak, and Kang L. Wang. Magnetization switching through giant spin–orbit torque in a magnetically doped topological insulator heterostructure. *Nat Mater*, 13(7):699–704, 07 2014.

[32] C. Ciccarelli, L. Anderson, V. Tshitoyan, A. J. Ferguson, F. Gerhard, C. Gould, L. W. Molenkamp, J. Gayles, J. Železný, L. Šmejkal, Z. Yuan, J. Sinova, F. Freimuth, and T. Jungwirth. Room-temperature spin–orbit torque in nimnsb. *Nature Physics*, 12:855 EP –, 05 2016.

[33] Ran Cheng, Jiang Xiao, Qian Niu, and Arne Brataas. Spin pumping and spin-transfer torques in antiferromagnets. *Phys. Rev. Lett.*, 113:057601, Jul 2014.

[34] J. Železný, H. Gao, K. Výborný, J. Zemen, J. Mašek, Aurélien Manchon, J. Wunderlich, Jairo Sinova, and T. Jungwirth. Relativistic néel-order fields induced by electrical current in antiferromagnets. *Phys. Rev. Lett.*, 113:157201, Oct 2014.

[35] Aurelien Manchon. Spin diffusion and torques in disordered antiferromagnets. *Journal of Physics: Condensed Matter*, 29(10):104002, 2017.

[36] Zhixin Qian and Giovanni Vignale. Spin dynamics from time-dependent spin-density-functional theory. *Phys. Rev. Lett.*, 88:056404, Jan 2002.

[37] V.M. Edelstein. Spin polarization of conduction electrons induced by electric current in two-dimensional asymmetric electron systems. *Solid State Communications*, 73(3):233 – 235, 1990.

[38] Arne Brataas and Kjetil M. D. Hals. Spin–orbit torques in action. *Nature Nanotechnology*, 9:86, 02 2014.

[39] J. Železný, H. Gao, Aurélien Manchon, Frank Freimuth, Yuriy Mokrousov, J. Zemen, J. Mašek, Jairo Sinova, and T. Jungwirth. Spin-orbit torques in locally and globally noncentrosymmetric crystals: Antiferromagnets and ferromagnets. *Phys. Rev. B*, 95:014403, Jan 2017.

[40] Guillaume Géranton, Bernd Zimmermann, Nguyen H. Long, Phivos Mavropoulos, Stefan Blügel, Frank Freimuth, and Yuriy Mokrousov. Spin-orbit torques and spin accumulation in fept/pt and co/cu thin films from first principles: The role of impurities. *Phys. Rev. B*, 93:224420, Jun 2016.

[41] S. Wimmer, K. Chadova, M. Seemann, D. Ködderitzsch, and H. Ebert. Fully relativistic description of spin-orbit torques by means of linear response theory. *Phys. Rev. B*, 94:054415, Aug 2016.

[42] V. P. Amin and M. D. Stiles. Spin transport at interfaces with spin-orbit coupling: Formalism. *Phys. Rev. B*, 94:104419, Sep 2016.

[43] Qing-feng Sun and X. C. Xie. Definition of the spin current: The angular spin current and its physical consequences. *Phys. Rev. B*, 72:245305, Dec 2005.

[44] Cong Xiao and Qian Niu. Semiclassical theory of spin-orbit torques in disordered multiband electron systems. *Phys. Rev. B*, 96:045428, Jul 2017.

[45] Jia Zhang, Julian P. Velev, Xiaoqian Dang, and Evgeny Y. Tsymbal. Band structure and spin texture of $bi_2se_3 3d$ ferromagnetic metal interface. *Phys. Rev. B*, 94:014435, Jul 2016.

[46] Papa B. Ndiaye, C. A. Akosa, M. H. Fischer, A. Vaezi, E.-A. Kim, and A. Manchon. Dirac spin-orbit torques and charge pumping at the surface of topological insulators. *Phys. Rev. B*, 96:014408, Jul 2017.

[47] M. Weiler, L. Dreher, C. Heeg, H. Huebl, R. Gross, M. S. Brandt, and S. T. B. Goennenwein. Elastically driven ferromagnetic resonance in nickel thin films. *Physical Review Letters*, 106(11):117601–, 03 2011.

[48] A. V. Scherbakov, A. S. Salasyuk, A. V. Akimov, X. Liu, M. Bombeck, C. Brüggemann, D. R. Yakovlev, V. F. Sapega, J. K. Furdyna, and M. Bayer. Coherent magnetization precession in ferromagnetic (ga,mn)as induced by picosecond acoustic pulses. *Physical Review Letters*, 105(11):117204–, 09 2010.

[49] Takehito Yokoyama, Jiadong Zang, and Naoto Nagaosa. Theoretical study of the dynamics of magnetization on the topological surface. *Phys. Rev. B*, 81:241410, Jun 2010.

[50] Yaroslav Tserkovnyak and Daniel Loss. Thin-film magnetization dynamics on the surface of a topological insulator. *Phys. Rev. Lett.*, 108(18):187201–, 04 2012.

[51] Mark H. Fischer, Abolhassan Vaezi, Aurelien Manchon, and Eun-Ah Kim. Spin-torque generation in topological insulator based heterostructures. *Phys. Rev. B*, 93:125303, Mar 2016.

[52] Farzad Mahfouzi, Branislav K. Nikolić, and Nicholas Kioussis. Antidamping spin-orbit torque driven by spin-flip reflection mechanism on the surface of a topological insulator: A time-dependent nonequilibrium green function approach. *Phys. Rev. B*, 93:115419, Mar 2016.

[53] Po-Hao Chang, Troels Markussen, Søren Smidstrup, Kurt Stokbro, and Branislav K. Nikolić. Nonequilibrium spin texture within a thin layer below the surface of current-carrying topological insulator bi_2se_3: A first-principles quantum transport study. *Phys. Rev. B*, 92:201406, Nov 2015.

[54] S. Ghosh and A. Manchon. Spin-orbit torque in a three-dimensional topological insulator–ferromagnet heterostructure: Crossover between bulk and surface transport. *Phys. Rev. B*, 97:134402, Apr 2018.

[55] Xiao-Liang Qi, Taylor L. Hughes, and Shou-Cheng Zhang. Topological field theory of time-reversal invariant insulators. *Phys. Rev. B*, 78:195424, Nov 2008.

[56] Kentaro Nomura and Naoto Nagaosa. Surface-quantized anomalous hall current and the magnetoelectric effect in magnetically disordered topological insulators. *Phys. Rev. Lett.*, 106:166802, Apr 2011.

[57] Hiroaki T. Ueda, Akihito Takeuchi, Gen Tatara, and Takehito Yokoyama. Topological charge pumping effect by the magnetization dynamics on the surface of three-dimensional topological insulators. *Phys. Rev. B*, 85:115110, Mar 2012.

[58] Joo-Von Kim, Robert E. Camley, and Robert L. Stamps. *Chapter Four - Spin-Torque Oscillators*, volume 63, pages 217–294. Academic Press, 2012.

[59] I. Dzyaloshinsky. A thermodynamic theory of "weak"ferromagnetism of antiferromagnetics. *Journal of Physics and Chemistry of Solids*, 4(4):241–255, 1958.

[60] Tôru Moriya. Anisotropic superexchange interaction and weak ferromagnetism. *Phys. Rev.*, 120:91–98, Oct 1960.

[61] Dimitrie Culcer, Jairo Sinova, N. A. Sinitsyn, T. Jungwirth, A. H. MacDonald, and Q. Niu. Semiclassical spin transport in spin-orbit-coupled bands. *Phys. Rev. Lett.*, 93:046602, Jul 2004.

[62] Di Xiao, Yugui Yao, Zhong Fang, and Qian Niu. Berry-phase effect in anomalous thermoelectric transport. *Phys. Rev. Lett.*, 97:026603, 2006.

[63] C L Dennis, R P Borges, L D Buda, U Ebels, J F Gregg, M Hehn, E Jouguelet, K Ounadjela, I Petej, I L Prejbeanu, and M J Thornton. The defining length scales of mesomagnetism: a review. *Journal of Physics: Condensed Matter*, 14(49):R1175–R1262, 2002.

[64] Kentaro Nomura and Naoto Nagaosa. Electric charging of magnetic textures on the surface of a topological insulator. *Phys. Rev. B*, 82:161401, Oct 2010.

[65] Xiao-Xiao Zhang, Andrey S. Mishchenko, Giulio De Filippis, and Naoto Nagaosa. Electric transport in three-dimensional skyrmion/monopole crystal. *Phys. Rev. B*, 94:174428, Nov 2016.

[66] S. E. Barnes and S. Maekawa. Generalization of faraday's law to include nonconservative spin forces. *Phys. Rev. Lett.*, 98:246601, Jun 2007.

[67] Frank Freimuth, Robert Bamler, Yuriy Mokrousov, and Achim Rosch. Phase-space berry phases in chiral magnets: Dzyaloshinskii-moriya interaction and the charge of skyrmions. *Phys. Rev. B*, 88:214409, 2013.

[68] F Freimuth, S Blügel, and Y Mokrousov. Berry phase theory of dzyaloshinskii-moriya interaction and spin-orbit torques. *Journal of Physics: Condensed Matter*, 26(10):104202, 2014.

[69] Frank Freimuth, Stefan Blügel, and Yuriy Mokrousov. The inverse thermal spin–orbit torque and the relation of the dzyaloshinskii–moriya interaction to ground-state energy currents. *Journal of Physics: Condensed Matter*, 28(31):316001, 2016.

[70] Frank Freimuth, Stefan Blügel, and Yuriy Mokrousov. Relation of the dzyaloshinskii-moriya interaction to spin currents and to the spin-orbit field. *Phys. Rev. B*, 96:054403, Aug 2017.

[71] Yang Gao, David Vanderbilt, and Di Xiao. Microscopic theory of spin toroidization in periodic crystals. *Phys. Rev. B*, 97:134423, Apr 2018.

[72] Anne S Zimmermann, Dennis Meier, and Manfred Fiebig. Ferroic nature of magnetic toroidal order. *Nature Communications*, 5:4796, 2014.

[73] Hua Chen, Qian Niu, and Allan H. MacDonald. Spin hall effect without spin currents in magnetic insulators. *arXiv:1803.01294*, 2018.

[74] Huei-Ru Fuh, Ching-Ray Chang, Yin-Kuo Wang, Richard F. L. Evans, Roy W. Chantrell, and Horng-Tay Jeng. Newtype single-layer magnetic semiconductor in transition-metal dichalcogenides vx2 (x = s, se and te). *Scientific Reports*, 6:32625 EP –, 09 2016.

[75] Wenwen Zhao, Bohua Dong, Zenglong Guo, Ge Su, Rongjie Gao, Wei Wang, and Lixin Cao. Colloidal synthesis of vse2 single-layer nanosheets as novel electrocatalysts for the hydrogen evolution reaction. *Chem. Commun.*, 52:9228–9231, 2016.

[76] Bevin Huang, Genevieve Clark, Efrén Navarro-Moratalla, Dahlia R. Klein, Ran Cheng, Kyle L. Seyler, Ding Zhong, Emma Schmidgall, Michael A. McGuire, David H. Cobden, Wang Yao, Di Xiao, Pablo Jarillo-Herrero, and Xiaodong Xu. Layer-dependent ferromagnetism in a van der waals crystal down to the monolayer limit. *Nature*, 546:270 EP –, 06 2017.

[77] Cheng Gong, Lin Li, Zhenglu Li, Huiwen Ji, Alex Stern, Yang Xia, Ting Cao, Wei Bao, Chenzhe Wang, Yuan Wang, Z. Q. Qiu, R. J. Cava, Steven G. Louie, Jing Xia, and Xiang Zhang. Discovery of intrinsic ferromagnetism in two-dimensional van der waals crystals. *Nature*, 546:265 EP –, 04 2017.

[78] Yang Gao, Shengyuan A. Yang, and Qian Niu. Field induced positional shift of bloch electrons and its dynamical implications. *Phys. Rev. Lett.*, 112:166601, Apr 2014.

[79] D. MacNeill, G. M. Stiehl, M. H. D. Guimaraes, R. A. Buhrman, J. Park, and D. C. Ralph. Control of spin–orbit torques through crystal symmetry in wte2/ferromagnet bilayers. *Nature Physics*, 13:300 EP –, 11 2016.

[80] Gui-Bin Liu, Wen-Yu Shan, Yugui Yao, Wang Yao, and Di Xiao. Three-band tight-binding model for monolayers of group-vib transition metal dichalcogenides. *Phys. Rev. B*, 88:085433, Aug 2013.

[81] Di Xiao, Junren Shi, Dennis P. Clougherty, and Qian Niu. Polarization and adiabatic pumping in inhomogeneous crystals. *Phys. Rev. Lett.*, 102:087602, Feb 2009.

Vita

Bangguo Xiong was born in Hubei, China in 1990. He received his Bachelor of Science degree in Physics from Peking University in 2012. After that he started to pursue a Ph.D in condensed matter physics in the University of Texas at Austin.

Permanent address: willyxq@gmail.com

This dissertation was typeset with LaTeX[†] by the author.

[†]LaTeX is a document preparation system developed by Leslie Lamport as a special version of Donald Knuth's TeX Program.